

Accepted Manuscript

Effective synthesis of benzimidazoles-imidazo[1,2-*a*]pyrazine conjugates: A comparative study of mono-and bis-benzimidazoles for antitumor activity

Iqbal Singh, Vijay Luxami, Kamaldeep Paul



PII: S0223-5234(19)30663-4

DOI: <https://doi.org/10.1016/j.ejmech.2019.07.042>

Reference: EJMECH 11539

To appear in: *European Journal of Medicinal Chemistry*

Received Date: 22 March 2019

Revised Date: 2 July 2019

Accepted Date: 12 July 2019

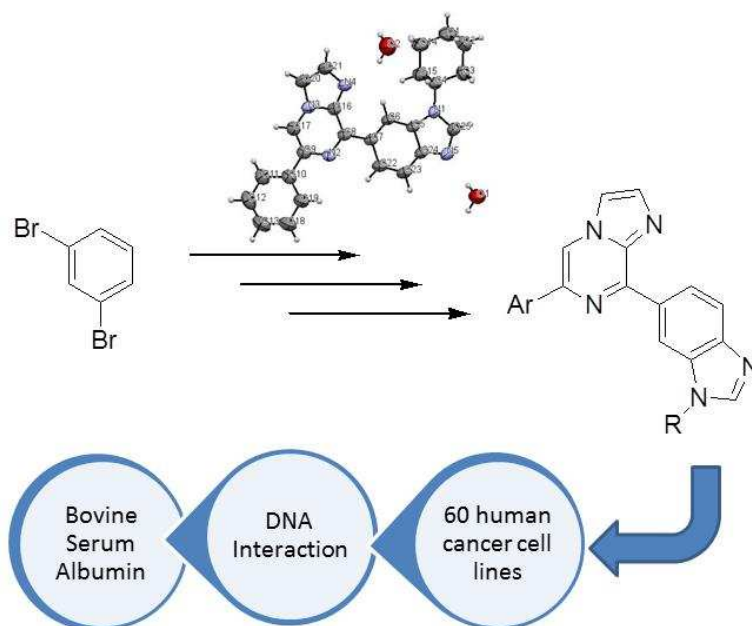
Please cite this article as: I. Singh, V. Luxami, K. Paul, Effective synthesis of benzimidazoles-imidazo[1,2-*a*]pyrazine conjugates: A comparative study of mono-and bis-benzimidazoles for antitumor activity, *European Journal of Medicinal Chemistry* (2019), doi: <https://doi.org/10.1016/j.ejmech.2019.07.042>.

This is a PDF file of an unedited manuscript that has been accepted for publication. As a service to our customers we are providing this early version of the manuscript. The manuscript will undergo copyediting, typesetting, and review of the resulting proof before it is published in its final form. Please note that during the production process errors may be discovered which could affect the content, and all legal disclaimers that apply to the journal pertain.

Effective synthesis of benzimidazoles-imidazo[1,2-*a*]pyrazine conjugates: A comparative study of mono- and bis-benzimidazoles for antitumor activity

Iqbal Singh, Vijay Luxami and Kamaldeep Paul*

School of Chemistry and Biochemistry, Thapar Institute of Engineering and Technology,
Patiala-147001, India



A novel series of imidazo[1,2-*a*]pyrazine-benzimidazole is first time synthesized and screen *in vitro* biological activity for 60 human cancer cell lines representing nine different cancer types.

Effective synthesis of benzimidazoles-imidazo[1,2-*a*]pyrazine conjugates: A comparative study of mono- and bis-benzimidazoles for antitumor activity

Iqbal Singh, Vijay Luxami and Kamaldeep Paul*

School of Chemistry and Biochemistry, Thapar Institute of Engineering and Technology, Patiala-147001, India

Email: kpaul@thapar.edu

ABSTRACT

A novel series of 6-substituted-8-(1-cyclohexyl-1*H*-benzo[*d*]imidazol-6-yl)imidazo[1,2-*a*]pyrazine and 6-substituted-8-(1-benzyl-1*H*-benzo[*d*]imidazol-6-yl)imidazo[1,2-*a*]pyrazine is first time synthesized and screen *in vitro* biological activity for 60 human cancer cell lines representing nine different cancer types. Derivatives **10** and **36** show antitumor activity for all tested cell lines, display comparable full panel mean-graph midpoint growth inhibition (MG_MID GI₅₀) values of 2.10 and 2.23 μ M, respectively. Furthermore, these derivatives show strong binding interactions with DNA and bovine serum albumin (BSA), studied through absorption, emission, and circular dichroism techniques. These spectroscopic studies reveal that imidazo[1,2-*a*]pyrazine- benzimidazoles **10** and **36**, intercalate with ct-DNA as a leading interaction for fundamental biologically significant effects, with monobenzimidazole show better activity than bisbenzimidazole. These experiments have confirmed that the imidazo[1,2-*a*]pyrazine and benzimidazole moieties are efficient pharmacophores to trigger binding to DNA. These compounds have also interacted with bovine serum albumin protein that demonstrating high values of binding constant.

Keywords: Imidazo[1,2-*a*]pyrazine; benzimidazole; anticancer activity; DNA interaction; bovine serum albumin

INTRODUCTION

DNA is one of the key targets for cytotoxic antiproliferative drugs. Generally, these antitumor agents damage DNA or block DNA synthesis, thus, responsible for inhibition of nucleic acid precursor biosynthesis, or disrupt hormonal stimulation of cell growth [1]. So, more efficient, less toxic, and target-specific non-covalently DNA binding anticancer drug needs to be developed. Extensive efforts have been currently centred on the development of new anticancer drugs based on combination of two active pharmacophores, particularly, bicyclic moieties, that are effective for binding and cleavage of DNA [2] under physiological conditions. The structures of benzimidazole and imidazo[1,2-*a*]pyrazine facilitate the compound bind strongly with DNA and hence, affect the critical metabolic routes. A large number of derivatives based on these moieties has been designed and evaluated for antitumor activity. Amongst these compounds, nocodazole, a 2-thienyl carbonyl benzimidazole, carbendazim [4], a benzimidazole carbamate and Veliparib [5], a pyrrolidine-2-yl benzimidazole are used in the clinic while mebendazole is currently undergoing clinical trials (**Figure-1**) [6]. The anticancer activity

of benzimidazoles appear to derive from their ability to form strong complexes with nucleic acids and thus induce DNA damage, and exert related effects such as topoisomerase poisoning, telomerase inhibition and inhibition of gene transcription [7-9]. Consequently, extensive studies on the mode and mechanism of interaction of benzimidazoles for binding to DNA are also reported from our laboratory. To regulate the interaction properties of the drugs, different substituents as well as new rings (quinazoline, triazine, purine, naphthalimide etc) were introduced with benzimidazole moiety (**Figure 1, A-D**) [10-13]. With these derivatives, pharmacological data showed that the maximum cytotoxicity was obtained with compounds substituted at position -5 or -6 of benzimidazole, and in particular with 2-chlorophenyl, 2-methoxyphenyl and pyrrolidine analogues. Additionally, it turned out that some of these compounds were evaluated towards cell lines and DNA, displayed positive activity on tumor and strong binding interactions with DNA. We anticipated that the proposed molecules with 6-substituted benzimidazole would also bind with DNA, and favour the interaction with nucleophilic sites of nucleic acid bases. Elucidation of the DNA binding activity of these analogues might provide a new array of seeking other pharmacological activities.

To check these binding interactions and antitumor activity, we studied more closely the chemical reactivity of imidazo[1,2-*a*]pyrazines-benzimidazole conjugates with variation of substitution at 6-position of imidazo[1,2-*a*]pyrazine. We have also prepared symmetrical and unsymmetrical benzimidazole substituted-imidazo[1,2-*a*]pyrazines, whereby compounds showed pronounced antitumor activity. It has been observed that the most promising compound inhibited tumor growth, which was related to their high DNA binding capacity, and the imidazo[1,2-*a*]pyrazine and benzimidazole substituted derivatives showed the prominent activity [14,15]. From all of the above-mentioned reflections, it has prompted us to prepare novel derivatives of 6-substituted-8-(1-cyclohexyl-1*H*-benzo[*d*]imidazol-6-yl)imidazo[1,2-*a*]pyrazine and 6-substituted-8-(1-benzyl-1*H*-benzo[*d*]imidazol-6-yl)imidazo[1,2-*a*]pyrazine (**Figure 2**), detailed study of their interactions with DNA, and antitumor activity on the panel of cancer cell lines.

At the same time, proteins have also attracted enormous research interest as a prime molecular target. Amongst the serum albumins, bovine serum albumin (BSA) is the most important protein present in plasma, carries several exo- and endogenous compounds [16]. Attention has now been centred on the protein required to drive and transportation of the drug to the target site for antitumor activity [17]. Thus, it is essential to explore drug-protein interaction, as most of the drugs bound to serum albumin are usually transported as a protein complex.

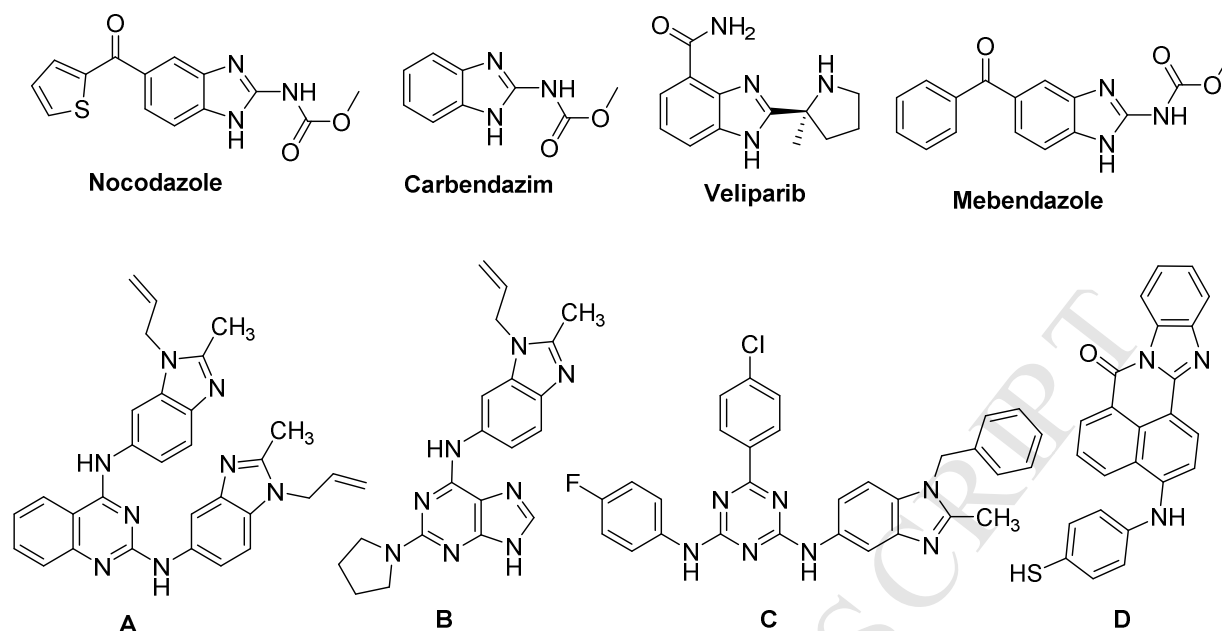


Figure 1. Structures of benzimidazole derivative

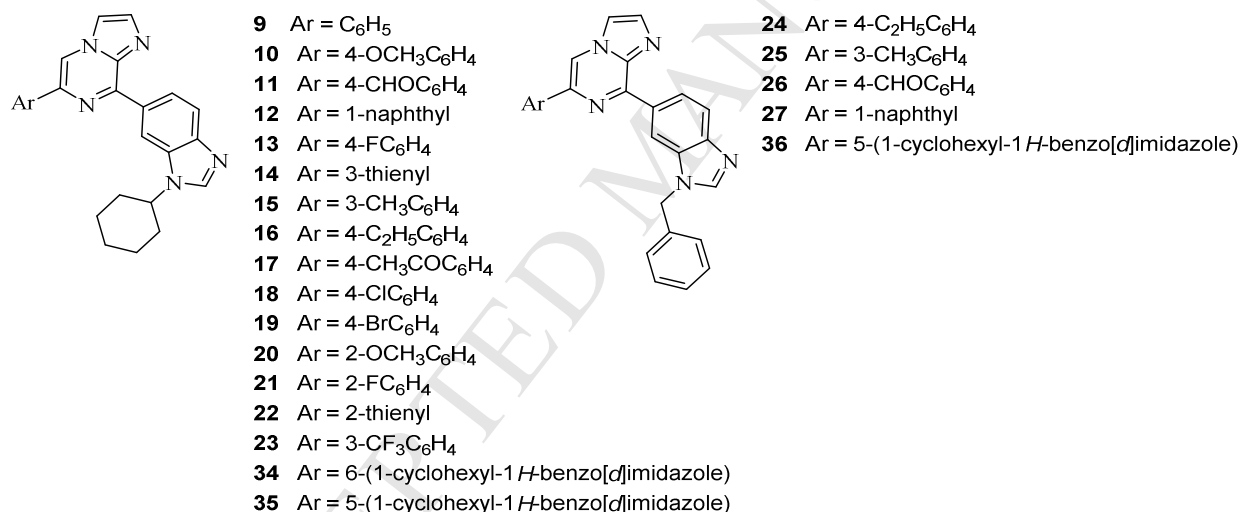


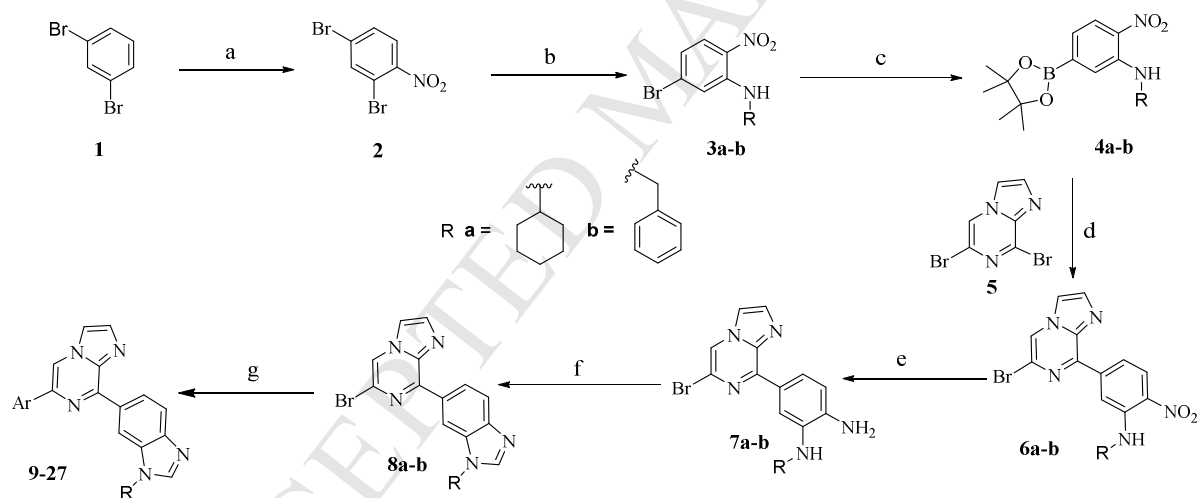
Figure 2. Derivatives of 6-substituted-8-(1-cyclohexyl-1*H*-benzo[*d*]imidazol-6-yl)imidazo[1,2-*a*]pyrazine and 6-substituted-8-(1-benzyl-1*H*-benzo[*d*]imidazol-6-yl)imidazo[1,2-*a*]pyrazine

RESULTS AND DISCUSSION

Chemistry: All compounds (**9-27** and **34-36**) shown in **Figure 2** were prepared according to the **Schemes 1-2** starting from 1,3-dibromobenzene (**Figures S1-S56**). The commercial available 1,3-dibromobenzene **1** was nitrated in the presence of sulphuric acid and nitric acid to afford **2** in 95% yield which was regioselectively substituted with cyclohexylamine and benzylamine in DMF, afforded **3a** and **3b**, respectively. Formation of **3a** was confirmed using NMR spectral analysis, with the multiplets of eleven protons corresponding to cyclohexyl ring in the range of δ 3.46-1.22 ppm. Boronation of **3a** and **3b** using bis(pinacolato)diboron in the presence of Pd(PPh₃)₂Cl₂ and KOAc

provided **4a** and **4b**, respectively. Characteristic signals of twelve protons of four methyl groups of boronate at δ 1.35 ppm, confirmed the formation of **4a**. Suzuki-Miyaura cross-coupling of **4a-b** with dibromo-imidazo[1,2-*a*]pyrazine **5** [18] and Pd(PPh₃)₄, afforded compound **6a-b** alongwith traces of disubstituted products. Disappearance of singlet of methyl groups at δ 1.35 ppm of boronate and appearance of aromatic protons of imidazo[1,2-*a*]pyrazine in the range of δ 8.69-7.77 ppm in ¹H NMR spectrum confirmed the formation of **6a**. Reduction of derivatives with sodium dithionite in ammonia provided amines **7a-b** followed by cyclization with triethylorthoformate in acetic acid to obtain intermediates **8a** and **8b** in 90% and 80% yields, respectively. Appearance of one additional proton at aromatic region confirmed the formation of compounds **8a** and **8b**. Derivatives **3b-7b** have not been separated from column chromatography and used further without purification. Suzuki reactions of intermediates with unsubstituted and substituted phenyl, thienyl and naphthyl boronates were carried out in CH₃CN:H₂O using Pd(PPh₃)₄ and K₂CO₃ afforded **9-27** in 75-85% yields (**Scheme 1, Figure S1**). Appearance of five protons of phenyl ring, three protons of imidazopyrazine and four protons of benzimidazole at aromatic region confirmed the formation of compound **9**.

Scheme 1. Synthesis of 6-substituted-8-(1-cyclohexyl-1*H*-benzo[*d*]imidazol-6-yl)imidazo[1,2-*a*]pyrazine^a

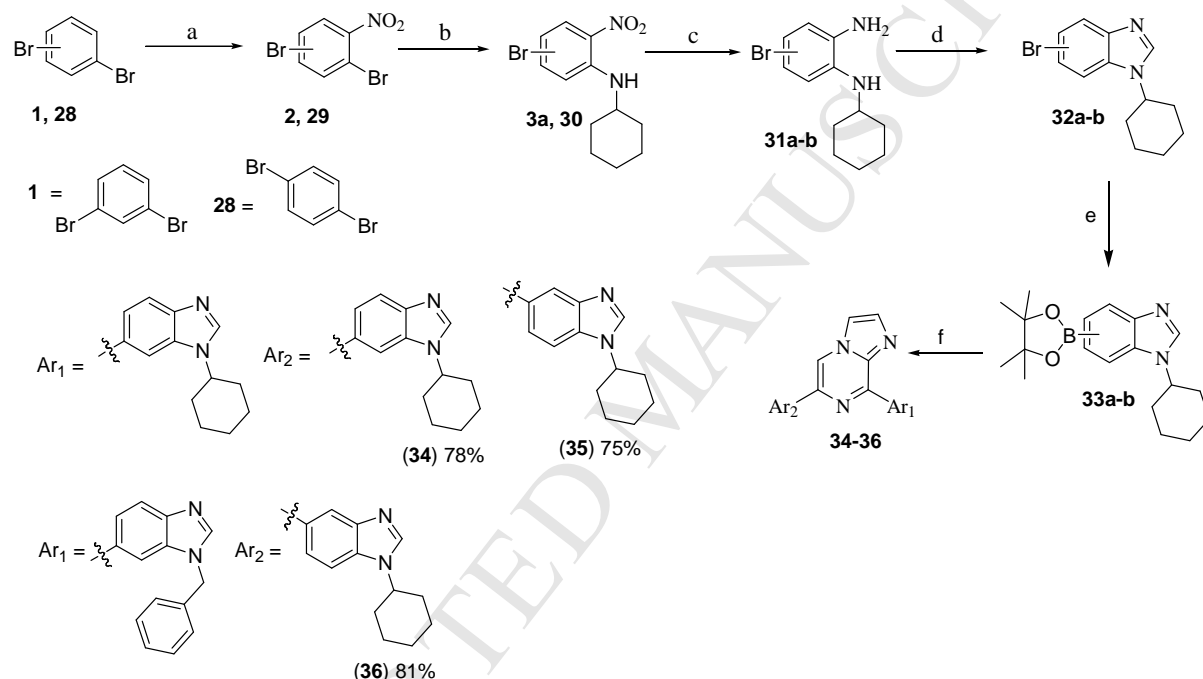


^aReagents and conditions: (a) H₂SO₄, HNO₃, DCM, 0 °C, 30 min., 95%; (b) Cyclohexyl amine/benzyl amine, K₂CO₃, DMF, 100 °C, 18 h; (c) Bis(pinacolato)diboron, Pd(PPh₃)₂Cl₂, KOAc, 1,4-dioxane, reflux, 10 h; (d) Pd(PPh₃)₄, K₂CO₃, CH₃CN : water (9:1), N₂, reflux, 10-12 h; (e) Na₂S₂O₄, aq. NH₃, THF : water, rt, 1 h; (f) Triethylorthoformate, AcOH, rt, 10 min., 80-90%; (g) ArB(OH)₂, Pd(PPh₃)₄, K₂CO₃, CH₃CN : water (9:1), N₂, reflux, 12-15 h, 75-85%.

Interestingly, the scope of another benzimidazole at C-6 position of imidazo[1,2-*a*]pyrazine for Suzuki reaction was also explored with different synthetic route (**Scheme 2**). Nitration of the commercial available 1,3- and 1,4-dibromobenzene (**1** and **28**) to yield **2** and **29**, respectively, which were substituted with cyclohexylamine in DMF, afforded **3a** and **30**. Formation of **30** was confirmed using NMR spectral analysis, by the multiplet of eleven protons, corresponding to cyclohexyl ring in the range of δ 3.52-1.25 ppm and broad singlet at δ 8.12 ppm of NH. Reductions of **3a** and **30** were

carried out with sodium dithionite in the presence of ammonia to afford **31a** and **31b**, respectively, followed by cyclization with triethylorthoformate in acetic acid, produced respective benzimidazoles **32a** and **32b**. Boronation of derivatives using bis(pinacolato)diboron in the presence of Pd(PPh₃)₂Cl₂ and KOAc afforded **33a** and **33b**. Suzuki-Miyaura cross-couplings of benzimidazole boronates **33a-b** with intermediate **8a-b** have been performed using Pd(PPh₃)₄ and K₂CO₃ to afford **34-36** in 75-81% yields. Appearance of three protons of imidazopyrazine and eight protons of benzimidazoles at aromatic region, and twenty two protons of two cyclohexyl rings at δ 3.42-1.31 ppm confirmed the formation of compound **34**.

Scheme 2. Synthesis of 6/8-(1-benzyl/cyclohexyl-1H-benzo[d]imidazol-5/6-yl)-6/8-(1-cyclohexyl-1H-benzo[d]imidazol-5/6-yl)imidazo[1,2-a]pyrazine^b



^bReagents and conditions: (a) H₂SO₄, HNO₃, DCM, 0 °C, 30 min., 93-95%; (b) Cyclohexyl amine, K₂CO₃, DMF, 100 °C, 18 h; (c) Na₂S₂O₄, aq. NH₃, THF : water (3:2), rt, 1 h; (d) Triethylorthoformate, AcOH, rt, 10 min.; (e) Bis(pinacolato)diboron, Pd(PPh₃)₂Cl₂, KOAc, 1,4-dioxane, reflux, 12 h; (f) **8a-b**, Pd(PPh₃)₄, K₂CO₃, CH₃CN : water (9:1), N₂, reflux, 10-12 h, 75-81%.

X-ray crystal structure. The molecular structure and the assignment of **9** were unambiguously confirmed by single-crystal X-ray diffraction study (**Figure 3, S57**).

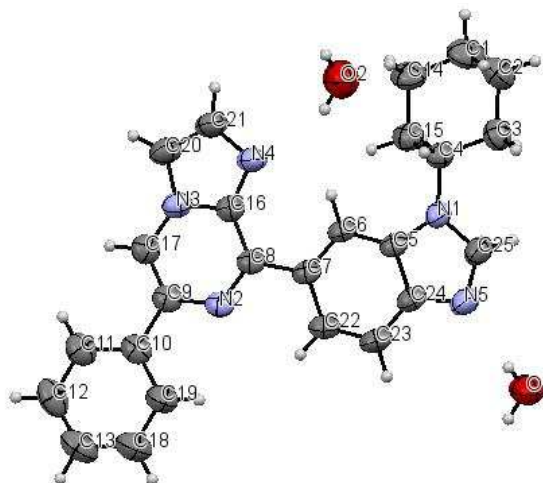


Figure 3. X-ray crystal structure of compound **9** (CCDC No. 1828636)

Compound **9** consists of two planar fragments, benzimidazole and imidazo[1,2-*a*]pyrazine which are in conjugation with phenyl ring present at C6-position of imidazo[1,2-*a*]pyrazine. Compound **9** crystallizes with $Z = 4$ in the space group P2/n (**Tables S2-S9**). Torsion angles along C-N and C-C of imidazo[1,2-*a*]pyrazine are 174.66 (13) Å and 5.0 (2) Å, respectively, while torsion angle along C-C bond of benzimidazole is 6.3 (2) Å. Moreover, the C-C bond length between imidazo[1,2-*a*]pyrazine and benzimidazole is shifted to double bond length (1.48 Å). The six membered cyclohexyl ring present at benzimidazole ring is deviated from planarity that exist in chair conformation. Atom systems C2-C1-C14 and C3-C4-C15 having angle strain, slightly deviated by 1.8° and 1.5°, respectively from the ideal tetrahedral value. The bond length of N5-C25 (1.31 Å) of benzimidazole ring is shorter having double bond character than longer bond length of N1-C25 (1.36 Å), indicating the presence of cyclohexyl group at N1 position and imidazo[1,2-*a*]pyrazine attached at the 6-position of benzimidazole (C7). Similarly, phenyl ring present at 6-position of imidazo[1,2-*a*]pyrazine having the bond length of 1.48 Å, indicating conjugation of these two moieties. Indeed, C-C bond length of imidazo[1,2-*a*]pyrazine with benzimidazole and phenyl ring agrees well with the standard double bond length of sp^2 hybridized carbon atoms in the rings. There is thus strong conjugation between these different planar moieties constitute the skeleton of molecule.

Molecular properties and drug-likeness. Good bioavailability can be achieved with appropriate balance between solubility and partitioning properties. We have subjected a series of imidazo[1,2-*a*]pyrazine-benzimidazole derivatives (**9-27** and **34-36**) for the prediction of lipophilicity and solubility with Lipinski's "Rule of Five" [19]. The results from the calculations revealed that all the derivatives fulfilled the Lipinski's rule except compounds **34-36**, in which violation was due to high molecular mass (**Table S10**). Experimental log P was determined by the octanol/water partition coefficient using UV-visible spectroscopy. All of the compounds showed log P values less than 5 indicating good lipophilicity to penetrate into the cell. Compounds possessed less number of rotatable bonds (3-5) and therefore, exhibited less conformational flexibility. These compounds showed Topological Polar Surface Area (TPSA) value of $< 70 \text{ \AA}^2$ that is also supported the drug absorption in

digestive tract as well as blood-brain barrier penetration [20,21]. Calculation of percentage oral absorption (%ABS = 109 - 0.345 TPSA) concluded that all derivatives were likely to be absorbed well, having calculated oral absorption in the range of 86-92%.

Biological studies. Antiproliferative activity. National Cancer Institute (NCI) has obtained samples from the NCI's panel of 60 human tumor cell lines and measured a variety of targets in these cell lines including gene mutations, mRNA levels, protein levels and enzyme activities. The compound might inhibit these targets, or, the compound interacts with a related target (maybe a component of the same metabolic pathway). The compound might cause some sort of damage that is repaired by the targets. The target might regulate genes whose products are inhibited by the compound. The compound might interact with a cellular component and trigger a checkpoint that requires the target, thus might kill the cell. In a preliminary test, compounds were assayed at single dose concentration (10^{-5} M) in the full panel of NCI 60 cancer cell lines [22]. The tested compounds showed diverse but strong antiproliferative effect on the evaluated panel of cell lines and most of the compounds exhibited more than 50% inhibition of tumor growth at micromolar concentration. As revealed from results of 21 tested compounds, six compounds with wide range of growth percentage displayed strong growth inhibitory activity (-88.03 to 99.61) at 10 μ M concentration (**Table 1**). The monobenzimidazole derivative **10** demonstrated superior activity than bisbenzimidazole with cytostatic effects towards 42 cell lines while later showed cytotoxic effect with 43 cancer cell lines (in case of compound **36**). Thus, amongst the monobenzimidazoles, 4-methoxyphenyl at C6 position of imidazo[1,2-*a*]pyrazine **10** indicated better cytostatic activity than phenyl **9**, 4-ethylphenyl **24** and 4-formylphenyl **26** derivatives in the series of compounds. Such findings denote that bisbenzimidazole moiety is more favorable for cytotoxic and mono benzimidazole for cytostatic activity. This superiority in the activity might be attributed to the corresponding increase in binding interactions through π bonding and therefore, permeability and penetration into cancer cells. On referring to the total number of sensitive cell lines for tested compounds, it has been found that most of the target compounds exhibited broad spectrum anti-tumor activity covering different cancer subpanels. Amongst these sensitive cell lines to tumor, colon cancer cell line HCC-2998 was found to be highly sensitive with negative growth percentage value (lethal effect) for derivative **36**. Central nervous system (SF-539) cancer cell lines were noticed to be the most susceptible cell lines for derivative **10**. Moreover, T-47D (breast cancer) was also proved to be the most responsible cells to compounds **9**, **24** and **26**. Compounds **10** and **36** attributed pronounced antitumor activity over the majority of tested cancer cell lines. The detailed anti-tumor activities on growth inhibition of NCI-60 human cancer cell lines at the single dose of 10 μ M, are shown in **Tables S11-S13**.

Table 1. Overview of the preliminary anticancer assay at single dose concentration of 10 μ M

Compd.	Mean growth	Range of growth inhibition	The most sensitive	Positive cytostatic	Positive cytotoxic	No. of sensitive cell lines/Total
--------	-------------	----------------------------	--------------------	---------------------	--------------------	-----------------------------------

	percent		cell lines	effect ^b	effect ^c	cell lines
9	59.72	-11.09 ^a to 92.04	T-47D	17/57	1/57	18/57
10	20.32	-43.35 ^a to 98.64	SF-539	42/57	9/57	51/57
24	65.98	0.55 to 94.82	T-47D	14/59	0/59	14/59
26	71.82	0.53 to 98.01	T-47D	9/59	0/59	9/59
34	54.67	7.04 to 89.11	RPMI-8226	24/59	0/59	24/59
36	-26.50	-88.03 ^a to 99.61	HCC-2998	16/59	43/59	59/59

^aNegative (-) indicates the cell killed. ^bThe ratio between number of cell lines with percent growth from 0 to 50 and total number of cell lines. ^cThe ratio between number of cell lines with percent growth of <0 and total number of cell lines.

Compounds **10** and **36** have been shown interesting growth inhibitory activity in the preliminary single dose screen and were evaluated for the advance 5-dose (10^{-4} - 10^{-8} M) testing mode against the full panel. In five dose assay, the monobenzimidazole derivative seemed to contribute better activity toward tumor growth which is evident from full panel mean-graph midpoint growth inhibition (MIG_MID GI₅₀) of compounds **10** (2.10 μ M) and **36** (2.23 μ M) (**Table-2**) as these values disguise significant cell selectivity. The mean GI₅₀ graph of 4-methoxyphenyl (**10**) showed potent activity in the leukemia, non-small cell lung, colon, CNS, renal, prostate and breast cancer subpanels. Compound **10** showed GI₅₀ of 422 nM for K-562 and 890 nM for SR of Leukemia cancer, GI₅₀ of 622 nM for NCI-H460 and 424 nM for NCI-H522 of non-small cell lung cancer, GI₅₀ of 399 nM for HCT-116, and 383 nM for HT29 cells of colon cancer, 361 nM for SF-295 of CNS cancer and 312 nM for MDA-MB-435 cell lines of melanoma. Compound **10** also showed selectivity to other panel of cell lines as shown in **Table S14**. Compound **36** showed GI₅₀ of 799 nM for 786-0 cancer cell lines corresponding to renal (**Table S15**). Higher LC₅₀ values of compounds (usually > 100 μ M) to most of the cell panels indicated their low toxicity profile.

Table 2. Median growth inhibitory (GI₅₀, μ M), total growth inhibitory (TGI, μ M) and median lethal concentrations (LC₅₀, μ M) of *in vitro* evaluation of compounds **10** and **36** against subpanel of human tumor cancer cell lines.

Compd	Activity (μ M)	I	II	III	IV	V	VI	VII	VIII	IX	MIG_MID ^a
10	GI ₅₀	1.60	1.65	1.24	1.18	6.95	3.04	1.30	0.84	1.11	2.10
	TGI	5.05	6.15	9.23	2.49	3.20	7.64	^b	^b	19.23	7.57
	LC ₅₀	^b									
36	GI ₅₀	1.91	2.18	1.97	2.11	2.00	2.46	3.01	2.50	1.95	2.23
	TGI	5.57	4.56	3.74	2.82	4.04	5.92	3.62	4.82	3.6	4.30
	LC ₅₀	^b	3.41	6.12	^b	^b	^b	^b	^b	^b	4.76

I, leukemia; II, non-small cell lung cancer; III, colon cancer; IV, CNS cancer; V, melanoma; VI, ovarian cancer; VII, renal cancer; VIII, prostate cancer; IX, breast cancer. ^a Full panel mean-graph midpoint (MIG_MID) (μM). ^b Compounds showed values $> 100 \mu\text{M}$.

Cytotoxicity against human normal cell line. To evaluate the safety, cytotoxicity effect of the two most potent compounds (**10** and **36**) was determined by means of colorimetric assay (MTT assay) against human normal cell line (Hek293) at 10^{-4} , 10^{-5} , 10^{-6} , 10^{-7} and 10^{-8} M concentrations. It has been observed that derivative **10** showed only 19.05%, 16.51%, 15.07%, 14.79% and 13.96% cytotoxicity to Hek293 cells whereas compound **36** exhibited 18.05%, 14.53%, 14.11%, 13.60% and 12.08% cytotoxicity to Hek293 cells at above said concentrations (**Figure 4**). Cytotoxicity data shown that compounds **10** and **36** have low cytotoxicity against mammalian cells, indicating the compounds were able to selectively kill the cancer cells.

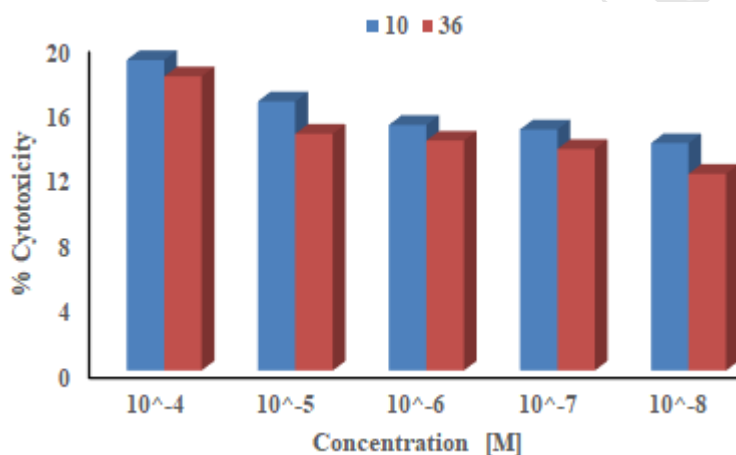


Figure 4. Effect of cytotoxicity of compounds **10** and **36** on human normal cell line Hek293

DNA interaction studies. The mode of anticancer activity of imidazo[1,2-*a*]pyrazine-benzimidazole conjugates might be grounded on DNA damage. Two most potent compounds **10** and **36** were studied with ct-DNA to investigate the effect of these compounds on antiproliferative activity. X-ray crystal structure analysis of these derivatives showed the planarity of compounds and previous studies performed with planar heterocycles had demonstrated for occurrence of an intercalative binding process upon complexation with DNA. So, these compounds might bound with DNA *via* intercalation. Here, we have studied the capacity of binding of imidazo[1,2-*a*]pyrazine-benzimidazole derivatives to DNA macromolecule with different spectroscopic methods like UV-visible, fluorescence and circular dichroism.

UV-visible spectroscopy. The absorption spectra of compounds **10** and **36** ($20 \mu\text{M}$) showed intense bands at 290 nm and 295 nm, respectively. On addition of ct-DNA ($0-15 \mu\text{M}$), hypochromic shifts were observed in phosphate buffer at *pH* 7.4. The absorbance of compounds **10** and **36** was decreased by 20.83% and 15.27%, respectively (**Figure 5a** and **S58**). During the titration with DNA, an isobestic point (**10**: 280 nm and **36**: 290 nm) was observed which suggested a single mode of binding

with compounds. Hypochromic effect observed in absorption spectra of compounds in the presence of ct-DNA is characteristic of an intercalative binding [23]. On the basis of interaction of compounds with DNA, the binding constants (K_b) for compound–DNA complexes have been determined from Benesi-Hildebrand equation (equation 1) [24] which were found to be $3.34 \pm 0.13 \times 10^4 \text{ M}^{-1}$ (95CI = 3.193 to 3.487 $\times 10^4$) for **10** and $3.18 \pm 0.01 \times 10^4 \text{ M}^{-1}$ (95CI = 3.169 to 3.191 $\times 10^4$) for **36** (Figure S59). These binding constants concluded that compound **10** has more affinity to bind with ct-DNA than **36**.

Any compound interacts with DNA, generally, interfere in the replication of DNA and stop the division of the cancer cells. So, strong DNA binding activity corresponds to the strong anticancer activity. In the present study, compound **10** interacted with DNA more strongly than compound **36**. Similarly, compound **10** ($GI_{50} = 2.10 \mu\text{M}$ for full panel mean-graph midpoint) showed more anticancer activity than compound **36** ($GI_{50} = 2.23 \mu\text{M}$ for full panel mean-graph midpoint) in 60 human cancer cell line studies, indicating the relationship of DNA-binding and anticancer activity.

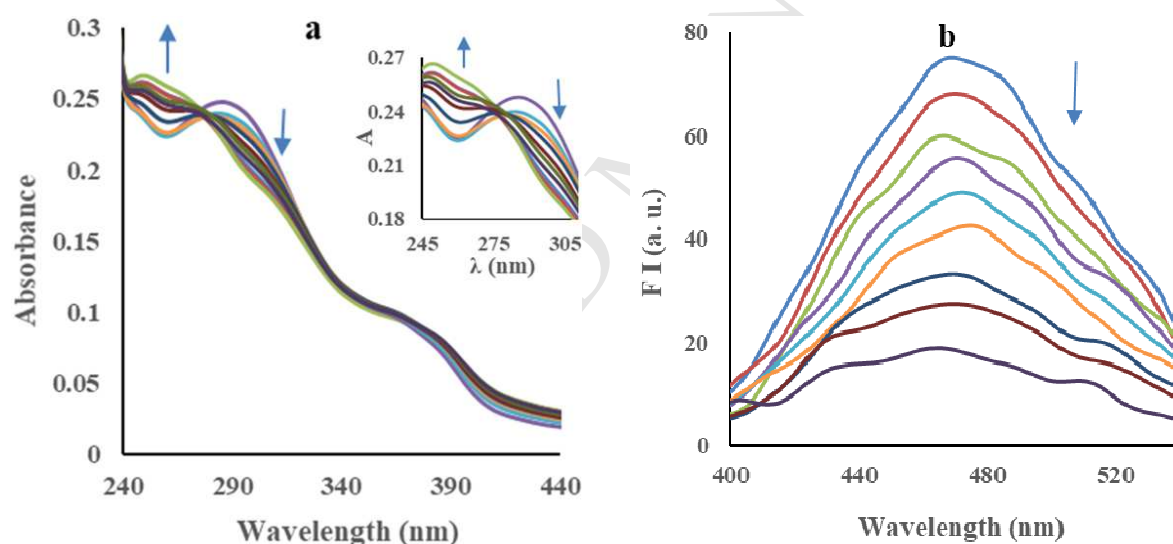


Figure 5. Effect of incremental addition of ct-DNA on (a) absorption and (b) emission spectra of compound **10** in phosphate buffer at pH 7.4.

Thermal denaturation studies. Thermal denaturation experiments were performed for further confirmation of interaction of compounds with DNA. The ability of the drug to protect ct-DNA against thermal denaturation was used as an indication of their capacity to bind DNA and to stabilize the double strand [25]. ΔT_m values for **10** and **36** on complexation with ct-DNA have been found to be 22 °C and 12 °C, respectively. ΔT_m values indicated that compound **10** has a strong affinity to bind with DNA due to less steric hindrance and thus stabilized DNA against heat denaturation.

Fluorescence spectroscopy. Emission studies provide additional information regarding the interaction mode of compounds with DNA. The binding of compounds with DNA was studied by

maintaining the concentration of compounds **10** and **36** at 5 μM while varying the concentration of ct-DNA (**10**: 0-110 μM ; **36**: 0-40 μM) in phosphate buffer (pH 7.4) at 298 K. On excitation of compounds **10** at 290 nm and **36** at 295 nm, showed intense emission bands at 470 and 450 nm, respectively. On increasing the concentration of ct-DNA to compounds, gradual quenching of the fluorescence intensities by 75% and 35%, for compounds **10** and **36**, respectively, were observed without any significant change in emission maxima (**Figures 5b** and **S60**). Stern Volmer equation (equation-2) [26] was performed to know more about the quenching process and to differentiate the probable quenching mechanism. K_{SV} was calculated from ratio of slope to intercept of Stern-Volmer plot (**Figure S61a**) and found to be $4.65 \pm 0.51 \times 10^4 \text{ M}^{-1}$ (95CI = 4.073 to 5.227×10^4) and $1.19 \pm 0.15 \times 10^4 \text{ M}^{-1}$ (95CI = 1.020 to 1.359×10^4) for **10** and **36**, respectively at 298 K (**Table 3**). Compound **10** had the more K_{SV} value, suggesting that compound **10** bound more strongly to ct-DNA than **36**.

A linear Stern-Volmer plot was obtained with compounds **10** and **36**, suggesting the possibility of single sort of binding process, either static or dynamic binding, which can be distinguished by bimolecular binding/quenching constant (K_q). The value of K_q was calculated using K_{SV} in equation 2 where the average fluorescence lifetime (τ_0) [27] is 10^{-8} s in the absence of DNA (analyte). The values of K_q were observed to be $4.65 \times 10^{12} \text{ M}^{-1} \text{ s}^{-1}$ and $1.19 \times 10^{12} \text{ M}^{-1} \text{ s}^{-1}$ for respective compounds **10** and **36** (**Table 3**) which are much greater than typically observed for dynamic enhancement ($\sim 1 \times 10^{10} \text{ M}^{-1} \text{ s}^{-1}$) [28]. The values of K_q indicated that interaction probably involved the static quenching with formation of complex at ground state.

Table 3. Quenching and binding parameters of compounds upon interaction with ct-DNA

Compds.	T (K)	$K_{SV} (\times 10^4) (\text{M}^{-1})$	$K_q (\times 10^{12}) (\text{M}^{-1} \text{s}^{-1})$	aR	$K_b (\times 10^4 \text{M}^{-1})$	n	bR
10	298	4.65	4.65	0.9567	36.52	1.29	0.9850
	308	1.68	1.68	0.9445	4.57	1.08	0.9614
	318	0.73	0.73	0.9669	0.02	0.58	0.9645
36	298	1.19	1.19	0.9921	9.58	1.21	0.9916

aR (K_{SV} and K_q) and bR (K_b and n) are the correlation coefficients

Modified Stern-Volmer equation (equation-3) [29] is generally used to calculate the binding constant (K_b) and the number of binding sites (n) and in the present study, were found to be $36.52 \pm 0.22 \times 10^4 \text{ M}^{-1}$ (95CI = 36.271 to 36.769×10^4) and 1.29 for compound **10** and $9.58 \pm 1.3 \times 10^4 \text{ M}^{-1}$ (95CI = 8.109 to 11.051×10^4) and 1.21 for compound **36** at 298 K (**Figure S61b**). Compound **10** showed 1.5 times more binding interaction than **36** suggested that **10** bound strongly to ct-DNA. To determine the effect of temperature on DNA binding with compounds, emission spectra of compound **10** (better binder with DNA) were recorded at 308 K and 318 K. On increasing the concentration of ct-DNA (308 K: 0-115 μM .; 318 K: 0-95 μM) to compound **10** (5 μM), there is gradual quenching of the fluorescence intensities by 65% and 60% at 308 K and 318 K, respectively, without any

significant change of wavelength in emission maxima (**Figure S62**). The values of the Stern-Volmer quenching constant [K_{SV} ; $1.68 \pm 0.32 \times 10^4 \text{ M}^{-1}$ (95CI = 1.318 to 2.042×10^4) and $0.73 \pm 0.08 \times 10^4 \text{ M}^{-1}$ (95CI = 0.515 to 0.945×10^4)], bimolecular quenching constant (K_q ; $1.68 \times 10^{12} \text{ M}^{-1} \text{ s}^{-1}$ and $0.7 \times 10^{12} \text{ M}^{-1} \text{ s}^{-1}$), the binding constant [K_b ; $4.57 \pm 0.16 \times 10^4 \text{ M}^{-1}$ (95CI = 4.389 to 4.751×10^4) and $0.02 \pm 0.005 \times 10^4 \text{ M}^{-1}$ (95CI = 0.014 to 0.026×10^4)] and the average number of binding site (n ; 1.08 and 0.58) were calculated at 308 K and 318 K (**Table 3, Figure S63**). A decrease in binding constant is observed with increasing temperature, indicating a reduction in the stability of the DNA-compound adduct at higher temperature with exothermic nature of the binding process.

Thermodynamic parameters were calculated for compound **10** according to the van't Hoff equation (equation 4) where enthalpy change (ΔH) and entropy change (ΔS) have been found to be -69.28 Kcal M^{-1} and -205.94 cal $\text{M}^{-1} \text{ K}^{-1}$, respectively (**Table 4, Figure S64**). The negative value of ΔH showed that binding process is exothermic. Accordingly, the negative values of ΔH and ΔS indicated that the hydrogen bonding and van der Waals contact played key role in the binding of compound to DNA [30]. Moreover, the negative values of ΔG obtained at different temperatures revealed the favourable spontaneous nature of the binding process. It is noteworthy that increase observed in ΔG value with temperature indicating the influence of temperature for interaction of compound with DNA.

Table 4. Thermodynamic parameters for the interaction of DNA with compound **10** at three different temperatures.

T (K)	ΔH (Kcal M^{-1})	ΔS (cal $\text{M}^{-1} \text{ K}^{-1}$)	ΔG (Kcal M^{-1})	aR
298	-69.28	-205.94	-7.91	0.9305
308			-5.85	
318			-3.79	

aR is the correlation coefficient

Ethidium bromide (EB) displacement. To evaluate the intercalation properties of compounds **10** and **36** with DNA, ethidium bromide (EB) displacement assay was performed. EB, a fluorescence probe, has a planar structure that simply binds with DNA by an intercalative binding mode [31]. The emission spectra of ethidium bromide-ct DNA complex ($3 \mu\text{M} : 30 \mu\text{M}$) at excitation of 520 nm, showed an intense band at 606 nm. The fluorescence intensity of EB-DNA complex at 606 nm decreased markedly with increasing the concentration of compounds ($0\text{-}85 \mu\text{M}$), indicated that some of the EB molecules, which were intercalated into DNA base pairs, have been replaced by compounds and released into the aqueous medium (**Figures 6a and S65**). The values of the Stern-Volmer quenching constant [K_{SV} ; $0.82 \pm 0.01 \times 10^4 \text{ M}^{-1}$ (95CI = 0.809 to 0.831×10^4) for compound **10** and $0.74 \pm 0.01 \times 10^4 \text{ M}^{-1}$ (95CI = 0.729 to 0.751×10^4) for compound **36**] and bimolecular quenching constant (K_q ; $0.82 \times 10^{12} \text{ M}^{-1} \text{ s}^{-1}$ for compound **10** and $0.74 \times 10^{12} \text{ M}^{-1} \text{ s}^{-1}$ for compound **36**) were calculated (**Figure S66**).

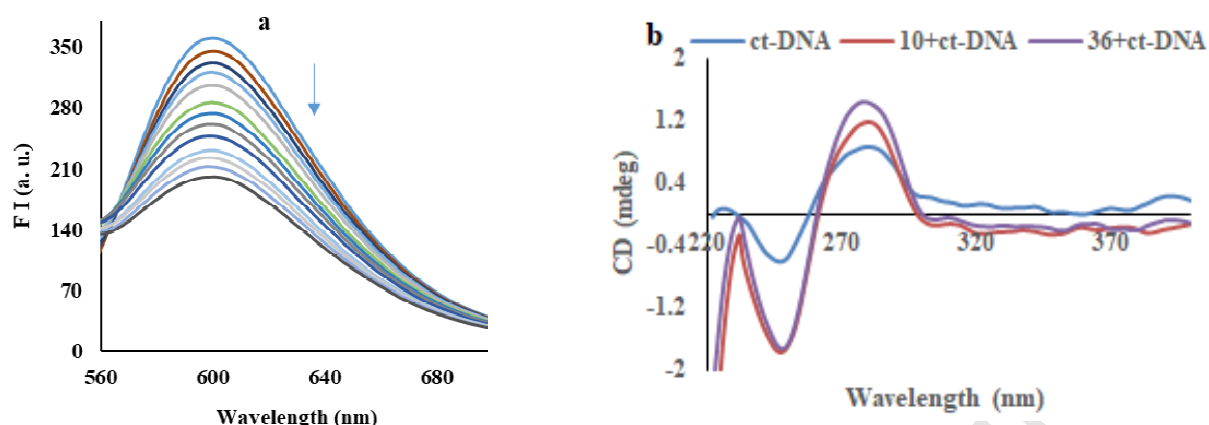


Figure 6. (a) Effect of incremental addition of compound **10** on emission spectrum of complex of EB ($3 \mu\text{M}$) and ct-DNA ($30 \mu\text{M}$); (b) CD spectra of free ct-DNA ($40 \mu\text{M}$) (blue line), **10**/ct-DNA complex (red line) and **36**/ct-DNA complex (purple line) at ratio $r_{[\text{compound}/\text{ct-DNA}]} = 0.025$.

Circular Dichroism (CD). In order to get insight into the conformation of ct-DNA on interaction with compounds, circular dichroism technique was used. The ct-DNA can eventually acquire induced CD spectrum (ICD) upon binding to molecules, from which mutual orientation of the ct-DNA could be derived, consequently giving useful information about mode of interaction. It was obvious that DNA had the characteristic CD signal in the UV-region, one negative band at 246 nm because of the right handed B-form helicity, and one positive band at 278 nm because of the base stacking [32] was observed. Addition of compounds **10** and **36** resulted in decrease in intensity of the ct-DNA, CD spectrum at (λ) 246 nm and increase of CD band at (λ) 278 nm (**Figure 6b**). These compounds yielded weak negative induced CD (ICD) band between (λ) 350 and 400 nm, thus excluding binding into the minor groove of ct-DNA as a dominant interaction. The results obtained for compounds **10** and **36** together with weak negative ICD band points toward intercalative binding mode of interaction with ct-DNA [33,34].

Bovine Serum Albumin (BSA) interactions. Serum albumin (SA) is the most abundant protein in plasma which involves in the transport of drugs within body. Binding to these proteins may lead to loss or enhancement of biological properties of the original drug. The possible binding interactions of compounds **10** and **36** with BSA, structural homology of human serum albumin (HSA), have been investigated by absorption and emission experiments.

UV-Visible spectroscopy. Absorption spectrum is a simple and appropriate technique to discover the structural changes of protein and to investigate the protein-ligand complex formation. Absorption spectra of BSA ($10 \mu\text{M}$) in phosphate buffer ($\text{pH } 7.4$) have been explored with incremental addition of compounds (**10** and **36**) at $0\text{--}8 \mu\text{M}$. The absorption band at 280 nm has been observed due to aromatic amino acids of BSA (Trp, Tyr, and Phe) which can be influenced by species that interact with this protein [35]. The intensity of the absorption peak of BSA has been increased markedly with increasing concentration of the compounds (**Figures 7a** and **S67**). These variations originated from

changes in the conformation and the polarity of the microenvironment around the aromatic residues of BSA. These, in turn, resulted from penetration of compounds into the structure of BSA.

The values of binding constant (K_b) for the interaction of compounds with BSA were used to compare the affinity of each derivative towards serum albumin. The binding constants (K_b) were calculated using Benesi-Hildebrand equation (equation 1) [24] by plot of $1/(A-A_0)$ versus $1/[\text{compound}]$ (**Figure S68**) from the ratio of the intercept to the slope and found to be $1.95 \pm 0.27 \times 10^5 \text{ M}^{-1}$ (95CI = 1.644 to 2.256×10^5) for **10** and $2.65 \pm 0.22 \times 10^4 \text{ M}^{-1}$ (95CI = 2.401 to 2.899×10^4) for **36**. Since the value of K_b is directly related to the extent of BSA binding and provide relative affinities, in the present study, indicating that monobenzimidazole derivatives (**10**) have more ability to penetrate into the cell than bisbenzimidazole moieties (**36**).

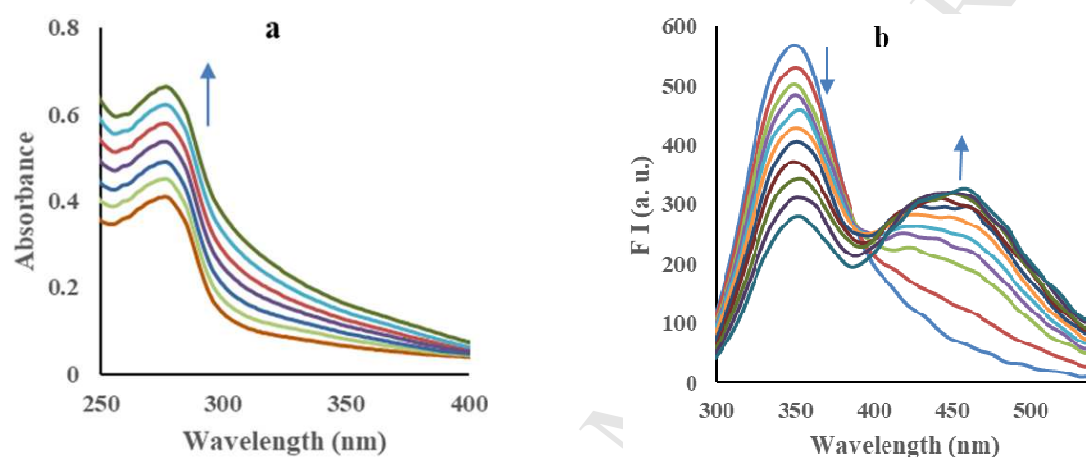


Figure 7. Effect of incremental addition of compound **10** on (a) absorption and (b) emission spectra of BSA ($10 \mu\text{M}$, phosphate buffer, $\text{pH } 7.4$).

Fluorescence spectroscopy. The effects of **10** and **36** on the emission of BSA have also been evaluated to gain more information on the interaction between the compounds and protein. Upon excitation at 280 nm, BSA exhibited an intense fluorescent emission band at around 350 nm mainly due to the presence of tryptophan residues. On increasing the concentration of compounds **10** (0-10 μM) and **36** (0-10 μM) to BSA ($10 \mu\text{M}$), quenching of the emission bands (75% for **36**) at 350 nm were observed, however, **10** showed ratiometric response toward BSA (**Figures 7b** and **S69**). The emission intensity ratio at 470/350 nm has been found to be changed from 0.08 to 1.08, clearly depicted the ~ 12 -fold ratiometric response indicating strong interaction of compound **10** with BSA.

A comparison has also been made for the binding affinity with the help of Stern-Volmer equation (equation-2) [26] that showed the relation between the quenching extent for each compound and the strength of their interactions with BSA. The values of Stern-Volmer constant (K_{SV}) and the apparent bimolecular quenching constant (K_q) were calculated to evaluate the efficiency of quenching and the accessibility of the fluorophores to the quenchers (compounds) (**Figure S70a**). A linear Stern-Volmer plot was obtained with derivatives suggesting that single sort of binding process occurs either static or

dynamic that can be distinguished by calculating bimolecular quenching constant (K_q) from equation-2 using the lifetime of the fluorophore (τ_0) [27] 10^{-8} s in the absence of the quencher (compound).

The values of K_{SV} for **10** and **36** were found to be $1.16 \pm 0.034 \times 10^5 \text{ M}^{-1}$ (95CI = 1.121 to 1.198 x 10^5) and $1.14 \pm 0.035 \times 10^5 \text{ M}^{-1}$ (95CI = 1.101 to 1.179 x 10^5), respectively. Compound **10** showed slightly higher value of K_{SV} than **36**, indicating that compound **10** has better affinity to bound with BSA. As shown in **Table 5**, the values of K_q for **10** and **36** have been found to be 1.16 and $1.14 \times 10^{13} \text{ M}^{-1}\text{s}^{-1}$, which are significantly larger than the diffusion-controlled limit ($\sim 1 \times 10^{10} \text{ M}^{-1} \text{ s}^{-1}$) [28], indicating binding of the compounds to BSA probably involves the static quenching with formation of complex at ground state.

The binding constants (K_b) and average number of binding sites (n) of imidazo[1,2-*a*]pyrazine-benzimidazole conjugates have been calculated using the modified Stern-Volmer equation (equation-3) [29] from plot of $\log(F_0-F)/F$ versus $\log[\text{compound}]$ (**Figure S70b**) and were found to be $4.68 \pm 0.017 \times 10^5 \text{ M}^{-1}$ (95CI = 4.661 to 4.699 x 10^5) and 1.50 for compound **10**, and $1.08 \pm 0.021 \times 10^5 \text{ M}^{-1}$ (95CI = 1.056 to 1.104 x 10^5) and 1.01 for compound **36**. Compound **10** showed the higher binding constant than **36**, indicating strong affinity with BSA. These binding parameters for the interactions suggested that serum albumins might act as carrier proteins for these compounds and their metabolites in delivering them to target tissues.

Table 5. Quenching and binding parameters for the interaction of BSA with compounds **10** and **36**

Compd	$K_{SV}(\times 10^5)(\text{M}^{-1})$	$K_q(\times 10^{13})(\text{M}^{-1}\text{s}^{-1})$	${}^a\text{R}$	$K_b(\times 10^5 \text{ M}^{-1})$	n	${}^b\text{R}$
10	1.16	1.16	0.9475	4.68	1.50	0.9700
36	1.14	1.14	0.9578	1.08	1.01	0.9771

${}^a\text{R}$ (K_{SV} and K_q) and ${}^b\text{R}$ (K_b and n) are the correlation coefficients

Molecular docking studies. Molecular docking is an important tool for researchers to speculate the interaction between potential drug (ligand) and biomolecules. In the present study, we have carried out docking using AutoDock suite (vina) [36] to confirm the mode of binding between compounds **10** and **36** with DNA (pdb 1BNA) [37]. The optimized cluster was ranked by energy levels in the best conformation of the ligand-DNA modelled structures, and the minimum binding energies of the DNA with compounds **10** and **36** have been found to be -10.7 and -9.3 Kcal/mol, respectively (**Table S16**). Methoxy group in case of **10** and N of benzimidazole in case of **36** are also involved in the H-bonding with purine moiety of the guanidine group. Hydrogen bond has been formed between the oxygen linked methoxy of **10** and H-22 hydrogen atom ($d = 2.5 \text{ \AA}$) association with N-2 of guanine (DG14 of the B chain). Similarly, compound **36** formed two hydrogen bonds with guanine. These hydrogen bonds were formed by the N of benzimidazole with the H-3 hydrogen atom ($d = 2.6 \text{ \AA}$) associated with N-3 of guanine (DG16 of B chain) and H-21 hydrogen atom ($d = 2.5 \text{ \AA}$) associated with N-2 of guanine (DG10 of A chain) (**Figure 8**). Hence, because of the strong π - π stacking interaction and the hydrogen bonding between compounds and the nucleic acid base, the

torsional motion of compounds reduces substantially in the DNA solution, leading to change in its emission yield.

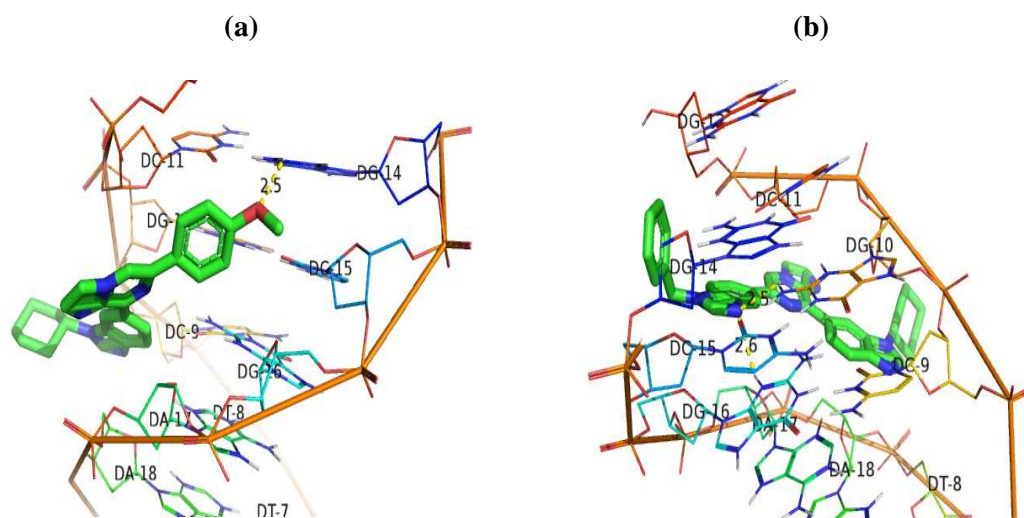


Figure 8. Molecular docking of DNA (1BNA) with compounds (a) **10** and (b) **36**, obtained from Discovery Studio.

CONCLUSION

Derivatives of new conjugated ring systems 6-substituted-8-(1-cyclohexyl-1*H*-benzo[*d*]imidazol-6-yl)imidazo[1,2-*a*]pyrazine and 6-substituted-8-(1-benzyl-1*H*-benzo[*d*]imidazol-6-yl)imidazo[1,2-*a*]pyrazine obtained in good to moderate yields from the key intermediate 6,8-dibromo-imidazo[1,2-*a*]pyrazine, exhibiting excellent cytotoxicity activity against about 60 human tumor cell lines with GI_{50} values reaching nanomolar concentrations in some of the cell lines. A particular efficacy was observed with monobenzimidazole derivative **10** against leukemia, colon, CNS and melanoma subpanels ($GI_{50} = 0.31\text{-}0.39 \mu\text{M}$). The results with DNA interactions suggested that the fluorescence of compounds **10** and **36** were quenched significantly and the probable quenching mechanism was a static quenching process. The binding mode of these compounds to DNA was an intercalation binding, which was supported by the results from ethidium bromide assay, circular dichroism and DNA-melting measurements. Interestingly, a satisfactory correlation was observed between the extent of DNA interaction and the antiproliferative activity. Moreover, the interaction of compounds **10** and **36** with bovine serum albumin proteins were studied through fluorescence emission spectroscopy that revealing the binding to BSA with relatively high stability constants ($K_b = 1.08\text{-}4.68 \times 10^5 \text{ M}^{-1}$) which rely between optimum range to suggest binding, transfer and release upon arrival at their targets. Thus, novel imidazo[1,2-*a*]pyrazine-benzimidazole conjugates with superior bioactivity profile and their mode of interactions with DNA have been described, and the objective is thus fully reached.

EXPERIMENTAL SECTION

Chemistry. *General Methods.* All commercially available compounds (Aldrich, Merck, Spectrochem etc.) were used without further purification. All the recorded melting points were uncorrected and measured in open capillaries. All ^1H and ^{13}C NMR characterization were performed on Jeol ECS 400 NMR spectrometer, which was operated at 400 MHz for ^1H nuclei and 100 MHz for ^{13}C nuclei, taking CDCl_3 as solvent. Chemical shifts are reported in parts per million (ppm) and TMS was used as an internal reference. Coupling constants (J) were reported in hertz (Hz). The synthesized compounds were characterized by mass spectra using Water Micromass-Q-T of Micro. Elemental analysis has been done with Thermo Scientific (Flash 2000) analyzer. Purification of synthesized compounds through column chromatography was done with the help of silica gel having mesh size of 60-120/100-200 using hexane/ethyl acetate and chloroform/methanol in various polarity system. UV-Vis studies were carried out on a Shimadzu UV-2600 machine using slit width of 1.0 nm and matched quartz cells. Emission spectra were determined on a Varian Cary Eclipse fluorescence spectrometer. CD spectra were carried out on Applied Photophysics CD spectrophotometer. Absorption and fluorescence scans were saved as ACS II files and further processed in ExcelTM to produce all graphs shown. Anticancer activities were evaluated at 9 panels of cancer cells including 60 different cancer cell lines at NCI, USA. These cancer cell lines are: panel (cell lines); Leukemia (CCRF-CEM, HL-60(TB), K-562, MOLT-4, RPMI-8226, SR), Non-Small Cell Lung Cancer (A549/ATCC, EXVX, HOP-62, HOP-92, NCI-H226, NCI-H23, NCI-H322M, NCI-H460, NCI-522), Colon Cancer (COLO 205, HCC-2998, HCT-116, HCT-15, HT29, KM12, SW-620), CNS Cancer (SF-268, SF-295, SF-539, SNB-19, SNB-75, U251), Melanoma (LOX IMVI, MALME-3M, M14, MDA-MB-435, SK-MEL-2, SK-MEL-28, SK-MEL-5, UACC-257, UACC-62), Ovarian Cancer (IGROV1, OVCAR-3, OVCAR-4, OVCAR-5, OVCAR-8, NCI/ADR-RES, SK-OV-3), Renal Cancer (786-0, A498, ACHN, CAKI-1, RXF 393, SN12C, TK-10, UO-31), Prostate Cancer (PC-3, DU-145), Breast Cancer (MCF7, MDA-MB-231/ATCC, HS 578T, BT-549, T-47D, MDA-MB-468).

2,4-dibromo-1-nitrobenzene (2) [38]: 1,3-Dibromobenzene (**1**) (5 gm, 21.18 mmol) in dichloromethane (15 ml) and sulphuric acid (10 ml) was treated with dropwise addition of cooled mixture of HNO_3 and H_2SO_4 (4:1) at 0°C and stirred for 30 min. Then, reaction was allowed to stir at room temperature. The reaction mixture was quenched by pouring into ice. The precipitated product was filtered and thoroughly washed with water. Air dried the crude to obtained the desired product (**2**) 5.53 gm, 95% yield; R_f 0.3 (hexane); mp 68-71 $^\circ\text{C}$.

5-Bromo-N-cyclohexyl/benzyl-2-nitroaniline (3a-b): 2,4-Dibromo-1-nitrobenzene (**2**) (3 gm, 10.71 mmol), cyclohexyl amine / benzyl amine (1.27 gm / 1.37 gm, 12.85 mmol) and potassium carbonate (1.47 gm, 10.71 mmol) were taken in dry dimethylformamide (20 ml) in 100 ml dried round bottom flask and stirred the reaction mixture for 18 h at 100°C . On completion of the reaction, 100 mL water was added to the reaction mixture at room temperature and extracted with ethyl acetate (3×50 mL). Extract was dried over anhydrous Na_2SO_4 , filtered and evaporation of solvent to get crude

product. Purification of the crude was done by column chromatography using hexane/ethyl acetate (20:1) as solvent system, to yield the desired product **3a-b**.

5-Bromo-N-cyclohexyl-2-nitroaniline (3a): Yellow solid; 2.36 gm, 74% yield; R_f 0.3 (hexane); mp 90-93 °C; ^1H NMR (CDCl_3 , 400 MHz): δ (ppm) 8.10 (d, $J = 7.00$ Hz, 1H, NH), 7.97 (d, $J = 9.12$ Hz, 1H, ArH), 6.97 (d, $J = 1.92$ Hz, 1H, ArH), 6.65 (dd, $^2J = 9.16$ Hz, $^3J = 2.04$ Hz, 1H, ArH), 3.46-3.39 (m, 1H, cyclohex-CH), 2.01-1.98 (m, 2H, cyclohex- CH_2), 1.78-1.74 (m, 2H, cyclohex- CH_2), 1.64-1.59 (m, 1H, cyclohex- CH_2), 1.45-1.22 (m, 5H, cyclohex- CH_2); ^{13}C NMR (CDCl_3 , 100 MHz): δ (ppm) 145.0, 131.6, 130.5, 128.6, 128.3, 118.2, 116.6 (ArC), 51.1 (CH), 32.6 (CH_2), 25.5 (CH_2), 24.5 (CH_2).

N-Cyclohexyl/benzyl-2-nitro-5-(4,4,5,5-tetramethyl-1,3,2-dioxaborolan-2-yl)aniline (4a-b): 5-Bromo-*N*-cyclohexyl/benzyl-2-nitroaniline (**3a-b**) (2 gm, 6.68 mmol), bis(pinacolato)diboron (2.03 gm / 1.99 gm, 8.01 mmol), potassium acetate (0.98 gm / 1.35 gm, 10.02 mmol), palladium(II)bis(triphenylphosphine)dichloride (1.0 mol%) and 1,4-dioxane (20 mL) were charged in an oven dried RBF. The reaction mixture was stirred at reflux condition for 10 h until the aryl halide was completely consumed as determined by thin layer chromatography. Solvent was evaporated under reduced pressure followed by addition of 100 ml of water into it. The crude product was extracted using chloroform (3 \times 50 mL). Extract was completely dried using anhydrous Na_2SO_4 and filtered to obtain the crude product. The product was purified *via* column chromatography using ethyl acetate and hexane as eluents to obtain desired product (**4a-b**).

N-Cyclohexyl-2-nitro-5-(4,4,5,5-tetramethyl-1,3,2-dioxaborolan-2-yl)aniline (4a): Reddish yellow solid; 1.80 gm, 78% yield; R_f 0.5 (10% ethylacetate in hexane); mp 120-122 °C; ^1H NMR (CDCl_3 , 400 MHz): δ (ppm) 8.10 (d, $J = 8.56$ Hz, 2H, NH & ArH), 7.26 (s, 1H, ArH), 6.94 (d, $J = 8.72$ Hz, 1H, ArH), 3.69-3.61 (m, 1H, cyclohex-CH), 2.03-2.00 (m, 2H, cyclohex- CH_2), 1.80-1.75 (m, 2H, cyclohex- CH_2), 1.65-1.61 (m, 1H, cyclohex- CH_2), 1.50-1.26 (m, 17H, cyclohex- CH_2 & boronate- CH_3); $^{13}\text{C}\{^1\text{H}\}$ NMR (CDCl_3 , 100 MHz): δ (ppm) 144.0, 135.7, 132.8, 125.8, 120.9, 120.1, (ArC), 84.5 (C), 50.4 (CH), 32.9 (CH_2), 25.0 (CH_2), 24.9 (CH_3), 24.4 (CH_2). MS (ESI): m/z 346.2 ($\text{M}^+ + 1$); Anal Calcd for $\text{C}_{18}\text{H}_{27}\text{BN}_2\text{O}_4$: C, 62.44; H, 7.86; N, 8.09; found C, 62.40; H, 7.80; N, 8.13.

5-(6-Bromoimidazo[1,2-a]pyrazin-8-yl)-N-cyclohexyl/benzyl-2-nitroaniline (6a-b): 3,6-Dibromoimidazo[1,2-*a*]pyrazine (**5**) (2 g, 7.22 mmol) in acetonitrile:water (9:1), *N*-cyclohexyl/benzyl-2-nitro-5-(4,4,5,5-tetramethyl-1,3,2-dioxaborolan-2-yl)aniline (**4a-b**) (2.49 gm / 2.58 gm, 7.22 mmol) and K_2CO_3 (1.0 g, 7.22 mmol) were added under inert atmosphere. Then, $\text{Pd}(\text{PPh}_3)_4$ (5 mol%) was added with continued nitrogen purging and refluxed the reaction for 10-12 h. The solvent was evaporated under reduced pressure followed by 50 ml water was added and extracted with chloroform. Chloroform layer was dried over sodium sulphate. Purification of the crude product was obtained by column chromatography by adopting hexane:ethylacetate (9:1) as eluents (**6a-b**).

5-(6-Bromoimidazo[1,2-a]pyrazin-8-yl)-N-cyclohexyl-2-nitroaniline (6a): Reddish solid; 2.09 gm, 70% yield; R_f 0.3 (10% ethylacetate in hexane); mp 152-154 °C; ^1H NMR (CDCl_3 , 400 MHz): δ (ppm) 8.67 (d, $J = 1.40$ Hz, 1H, ArH), 8.30 (s, 1H, ArH), 8.28 (d, $J = 9.08$ Hz, 1H, ArH), 8.20 (d, $J = 7.08$ Hz, 1H, NH), 7.87 (d, $J = 0.64$ Hz, 1H, ArH), 7.80 (dd, $^2J = 9.08$ Hz, $^3J = 1.72$ Hz, 1H, ArH), 7.75 (d, $J = 0.68$ Hz, 1H, ArH), 3.79-3.69 (m, 1H, cyclohex-CH), 2.21-2.15 (m, 2H, cyclohex- CH_2), 2.04-1.99 (m, 2H, cyclohex- CH_2), 1.83-1.76 (m, 3H, cyclohex- CH_2), 1.69-1.61 (m, 2H, cyclohex- CH_2), 1.54-1.43 (m, 1H, cyclohex- CH_2); $^{13}\text{C}\{^1\text{H}\}$ NMR (CDCl_3 , 100 MHz): δ (ppm) 147.3, 144.5, 144.0, 141.2, 136.6, 126.9, 125.9, 120.9, 120.1, 119.2, 117.4, 115.2, 114.1 (ArC), 51.4 (CH), 31.5 (CH_2), 25.6 (CH_2), 24.9 (CH_2).

5-(6-Bromoimidazo[1,2-a]pyrazin-8-yl)-N¹-cyclohexyl/benzylbenzene-1,2-diamine (7a-b): Round bottom flask was charged with 5-(6-bromoimidazo[1,2-a]pyrazin-8-yl)-N-cyclohexyl/benzyl-2-nitroaniline (**6a-b**) (2 gm, 4.80 mmol) and sodium dithionite (4.18 gm / 4.10 gm, 24.03 mmol) in THF:Water (3:2) mixture. Ammonia solution (5 ml) was added to stirred reaction and further stirred at room temperature for 1h. The reaction mixture was extracted with ethyl acetate. Ethyl acetate layer was dried over sodium sulphate. Crude brown product obtained was directly used for further reaction without purification.

6-Bromo-8-(1-cyclohexyl/benzyl-1H-benzo[d]imidazol-6-yl)imidazo[1,2-a]pyrazine (8a-b): 5-(6-Bromoimidazo[1,2-a]pyrazin-8-yl)-N¹-cyclohexyl/benzylbenzene-1,2-diamine (**7a-b**) (**7**) (1 gm, 2.59 mmol) was stirred with triethylorthoformate (0.385 gm / 0.375 gm, 2.59 mmol) in acetic acid at room temperature for 10 min. Reaction was quenched in water and treated with NaHCO_3 to basify the reaction and extracted using chloroform. Sodium sulphate was used to dry the chloroform layer. Purification of crude product was done through column chromatography using ethyl acetate and hexane (3:7) as eluents.

6-Bromo-8-(1-cyclohexyl-1H-benzo[d]imidazol-6-yl)imidazo[1,2-a]pyrazine (8a): Light brown solid; 0.91 gm, 90% yield; R_f 0.5 (40% ethylacetate in hexane); mp 175-178 °C; ^1H NMR (CDCl_3 , 400 MHz): δ (ppm) 9.00 (d, $J = 1.52$, 1H, ArH), 8.72 (dd, $^2J = 8.68$ Hz, $^3J = 1.72$ Hz, 1H, ArH), 8.23 (s, 1H, ArH), 8.11 (s, 1H, ArH), 7.93 (d, $J = 8.52$ Hz, 1H, ArH), 7.88 (d, $J = 1.16$ Hz, 1H, ArH), 7.72 (d, $J = 1.20$ Hz, 1H, ArH), 4.44-4.36 (m, 1H, cyclohex-CH), 2.30 (d, $J = 11.44$ Hz, 2H, cyclohex- CH_2), 2.01 (d, $J = 13.80$ Hz, 2H, cyclohex- CH_2), 1.88-1.78 (m, 3H, cyclohex- CH_2), 1.64-1.53 (m, 2H, cyclohex- CH_2), 1.43-1.28 (m, 1H, cyclohex- CH_2); $^{13}\text{C}\{^1\text{H}\}$ NMR (CDCl_3 , 100 MHz): δ (ppm) 149.6, 145.8, 142.3, 138.7, 136.0, 133.5, 129.5, 124.2, 122.6, 120.0, 117.7, 114.0, 112.6 (ArC), 55.3 (CH), 33.6 (CH_2), 25.7 (CH_2), 25.4 (CH_2). MS (ESI): m/z 395.0 ($\text{M}^+ + 1$); Anal Calcd for $\text{C}_{19}\text{H}_{18}\text{BrN}_5$: C, 57.59; H, 4.58; N, 17.67; found C, 57.48; H, 4.70; N, 17.93.

8-(1-Benzyl-1H-benzo[d]imidazol-6-yl)-6-bromoimidazo[1,2-a]pyrazine (8b): Light brown solid; 0.77 gm, 80% yield; R_f 0.4 (40% ethylacetate in hexane); mp 182-185 °C; ^1H NMR (CDCl_3 , 400 MHz): δ (ppm) 8.99 (d, $J = 1.40$ Hz, 1H, ArH), 8.71 (dd, $^2J = 8.68$ Hz, $^3J = 1.36$ Hz, 1H, ArH),

8.20 (s, 1H, ArH), 8.00 (s, 1H, ArH), 7.95 (d, $J = 8.72$ Hz, 1H, ArH), 7.85 (d, $J = 0.92$ Hz, 1H, ArH), 7.70 (d, $J = 0.92$ Hz, 1H, ArH), 7.37-7.28 (m, 5H, ArH), 5.48 (s, 2H, CH₂-benzyl); ¹³C{¹H} NMR (CDCl₃, 100 MHz): δ (ppm) 149.4, 145.9, 144.9, 138.6, 135.9, 135.2, 134.0, 129.9, 129.0, 128.3, 127.5, 124.2, 122.5, 120.1, 117.5, 113.8, 112.5 (ArC), 48.9 (CH₂-benzyl). MS (ESI): m/z 403.0 ($M^+ + 1$); Anal Calcd for C₂₀H₁₄BrN₅: C, 59.42; H, 3.49; N, 17.32; found C, 59.48; H, 3.60; N, 17.13.

6-Aryl-8-(1-cyclohexyl/benzyl-1H-benzo[d]imidazol-6-yl)imidazo[1,2-a]pyrazine (9-27):

6-Bromo-8-(1-cyclohexyl/benzyl-1H-benzo[d]imidazol-6-yl)imidazo[1,2-a]pyrazine (**8a-b**) (150 mg, 0.378 mmol), arylboronic acid (0.378 mmol), K₂CO₃ (52.27 mg, 0.378 mmol) and Pd(PPh₃)₄ (5 mol%) were taken in a mixture of acetonitrile : water (9:1). Reaction mixture was refluxed for 12-15 h under nitrogen until the completion of the reaction (checked by TLC). Solvents were evaporated under reduced pressure. Water (50 ml) was added to the mixture and extracted with chloroform. Chloroform layer was dried over sodium sulphate to get the crude product. Crude was further purified by column chromatography using hexane:ethylacetate as eluents.

8-(1-Cyclohexyl-1H-benzo[d]imidazol-6-yl)-6-phenylimidazo[1,2-a]pyrazine (9): Light green solid; 111.64 mg, 85% yield; R_f 0.5 (40% ethylacetate in hexane); mp 194-196 °C; ¹H NMR (CDCl₃, 400 MHz): δ (ppm) 9.18 (s, 1H, ArH), 8.79 (dd, ² $J = 8.60$ Hz, ³ $J = 1.48$ Hz, 1H, ArH), 8.37 (s, 1H, ArH), 8.10 (s, 1H, ArH), 8.05 (d, $J = 7.44$ Hz, 2H, ArH), 7.95 (d, $J = 8.60$ Hz, 1H, ArH), 7.83 (s, 1H, ArH), 7.73 (s, 1H, ArH), 7.51 (t, $J = 7.36$ Hz, 2H, ArH), 7.42 (t, $J = 7.12$ Hz, 1H, ArH), 4.42-4.34 (m, 1H, cyclohex-CH), 2.28 (d, $J = 12.04$ Hz, 2H, cyclohex-CH₂), 1.98 (d, $J = 11.36$ Hz, 2H, cyclohex-CH₂), 1.87-1.77 (m, 3H, cyclohex-CH₂), 1.60-1.51 (m, 2H, cyclohex-CH₂), 1.38-1.27 (m, 1H, cyclohex-CH₂); ¹³C{¹H} NMR (CDCl₃, 100 MHz): δ (ppm) 148.8, 145.4, 142.0, 138.9, 138.7, 136.7, 135.1, 133.4, 130.9, 128.9, 128.6, 126.2, 123.8, 119.8, 114.4, 113.7, 112.7 (ArC), 55.4 (CH), 33.5 (CH₂), 25.7 (CH₂), 25.5 (CH₂); MS (ESI): m/z 394.3 ($M^+ + 1$); Anal Calcd for C₂₅H₂₃N₅: C, 76.31; H, 5.89; N, 17.80; found C, 76.42; H, 5.87; N, 17.94.

8-(1-Cyclohexyl-1H-benzo[d]imidazol-6-yl)-6-(4-methoxyphenyl)imidazo[1,2-a]pyrazine (10): Light green solid; 121.76 mg, 76% yield; R_f 0.6 (40% ethylacetate in hexane); mp 196-198 °C; ¹H NMR (CDCl₃, 400 MHz): δ (ppm) 9.17 (d, $J = 1.04$, 1H, ArH), 8.76 (dd, ² $J = 8.56$ Hz, ³ $J = 1.40$ Hz, 1H, ArH), 8.33 (s, 1H, ArH), 8.10 (s, 1H, ArH), 8.01 (d, $J = 8.84$ Hz, 2H, ArH), 7.94 (d, $J = 8.64$ Hz, 1H, ArH), 7.83 (d, $J = 0.68$ Hz, 1H, ArH), 7.73 (d, $J = 0.64$ Hz, 1H, ArH), 7.03 (d, $J = 8.84$ Hz, 2H, ArH), 4.43-4.35 (m, 1H, cyclohex-CH), 3.86 (s, 3H, CH₃), 2.30 (d, $J = 11.60$ Hz, 2H, cyclohex-CH₂), 1.99 (d, $J = 13.60$ Hz, 2H, cyclohex-CH₂), 1.88-1.78 (m, 3H, cyclohex-CH₂), 1.62-1.52 (m, 2H, cyclohex-CH₂), 1.40-1.33 (m, 1H, cyclohex-CH₂); ¹³C{¹H} NMR (CDCl₃, 100 MHz): δ (ppm) 160.2, 148.9, 141.9, 138.9, 138.7, 135.1, 133.5, 131.0, 129.4, 127.6, 123.8, 119.9, 114.3, 114.2, 112.6, 112.6 (ArC), 55.5 (CH), 55.4 (OCH₃), 33.6 (CH₂), 25.7 (CH₂), 25.5 (CH₂); MS (ESI): m/z 424.3 ($M^+ + 1$); Anal Calcd for C₂₆H₂₅N₅O: C, 73.74; H, 5.95; N, 16.54; found C, 73.67; H, 5.78; N, 16.48.

4-(8-(1-Cyclohexyl-1H-benzo[d]imidazol-6-yl)imidazo[1,2-a]pyrazin-6-yl)benzaldehyde (11): Light green solid; 130.75 mg, 82% yield; R_f 0.4 (40% ethylacetate in hexane); mp 198-201 °C; ^1H NMR (CDCl_3 , 400 MHz): δ (ppm) 10.07 (s, 1H, CHO), 9.21 (s, 1H, ArH), 8.77 (dd, $^2J = 8.52$ Hz, $^3J = 1.36$ Hz, 1H, ArH), 8.54 (s, 1H, ArH), 8.26 (d, $J = 8.24$ Hz, 2H, ArH), 8.10 (s, 1H, ArH), 8.01 (d, $J = 8.32$ Hz, 2H, ArH), 7.95 (d, $J = 8.64$ Hz, 1H, ArH), 7.89 (d, $J = 0.80$ Hz, 1H, ArH), 7.81 (d, $J = 0.64$ Hz, 1H, ArH), 4.43-4.35 (m, 1H, cyclohex-CH), 2.31 (d, $J = 11.20$ Hz, 2H, cyclohex- CH_2), 2.01-1.97 (m, 2H, cyclohex- CH_2), 1.90-1.79 (m, 3H, cyclohex- CH_2), 1.63-1.52 (m, 2H, cyclohex- CH_2), 1.40-1.29 (m, 1H, cyclohex- CH_2); $^{13}\text{C}\{^1\text{H}\}$ NMR (CDCl_3 , 100 MHz): δ (ppm) 191.9 (CO), 149.4, 142.6, 139.0, 137.3, 136.2, 135.6, 130.5, 130.4, 126.7, 123.7, 120.1, 114.9, 114.7, 112.8 (ArC), 55.5 (CH), 33.6 (CH_2), 25.7 (CH_2), 25.5 (CH_2); MS (ESI): m/z 422.5 ($\text{M}^+ + 1$); Anal Calcd for $\text{C}_{26}\text{H}_{23}\text{N}_5\text{O}$: C, 74.09; H, 5.50; N, 16.62; found C, 74.42; H, 5.25; N, 16.57.

8-(1-Cyclohexyl-1H-benzo[d]imidazol-6-yl)-6-(naphthalen-1-yl)imidazo[1,2-a]pyrazine (12): Light green solid; 137.59 mg, 82% yield; R_f 0.4 (40% ethylacetate in hexane); mp 200-203 °C; ^1H NMR (CDCl_3 , 400 MHz): δ (ppm) 9.07 (d, $J = 1.12$ Hz, 1H, ArH), 8.80 (dd, $^2J = 8.60$ Hz, $^3J = 1.40$ Hz, 1H, ArH), 8.29-8.27 (m, 2H, ArH), 8.08 (s, 1H, ArH), 7.96 (d, $J = 7.08$ Hz, 1H, ArH), 7.92 (s, 1H, ArH), 7.90 (d, $J = 8.64$ Hz, 1H, ArH), 7.80 (d, $J = 0.52$ Hz, 1H, ArH), 7.70 (dd, $^2J = 6.96$ Hz, $^3J = 0.84$ Hz, 1H, ArH), 7.58-7.53 (m, 2H, ArH), 7.53-7.47 (m, 2H, ArH), 4.38-4.30 (m, 1H, cyclohex-CH), 2.27 (d, $J = 11.44$ Hz, 2H, cyclohex- CH_2), 1.96 (d, $J = 13.64$ Hz, 2H, cyclohex- CH_2), 1.85-1.75 (m, 3H, cyclohex- CH_2), 1.55-1.46 (m, 2H, cyclohex- CH_2), 1.34-1.25 (m, 1H, cyclohex- CH_2); $^{13}\text{C}\{^1\text{H}\}$ NMR (CDCl_3 , 100 MHz): δ (ppm) 148.9, 142.0, 140.3, 138.7, 135.3, 135.2, 134.1, 133.5, 131.8, 130.9, 129.4, 128.5, 127.7, 126.5, 126.1, 125.9, 125.4, 124.2, 119.9, 117.2, 114.2, 112.5 (ArC), 55.4 (CH), 33.5 (CH_2), 25.7 (CH_2), 25.4 (CH_2); MS (ESI): m/z 444.5 ($\text{M}^+ + 1$); Anal Calcd for $\text{C}_{29}\text{H}_{25}\text{N}_5$: C, 78.53; H, 5.68; N, 15.79; found C, 78.23; H, 5.89; N, 15.49.

8-(1-Cyclohexyl-1H-benzo[d]imidazol-6-yl)-6-(4-fluorophenyl)imidazo[1,2-a]pyrazine (13): Light green solid; 121.42, 75% yield; R_f 0.5 (40% ethylacetate in hexane); mp 186-188 °C; ^1H NMR (CDCl_3 , 400 MHz): δ (ppm) 9.18 (d, $J = 1.20$ Hz, 1H, ArH), 8.74 (dd, $^2J = 8.56$ Hz, $^3J = 1.48$ Hz, 1H, ArH), 8.35 (s, 1H, ArH), 8.09 (s, 1H, ArH), 8.04 (d, $J = 5.36$ Hz, 1H, ArH), 8.02 (d, $J = 5.32$ Hz, 1H, ArH), 7.94 (d, $J = 8.64$ Hz, 1H, ArH), 7.84 (s, 1H, ArH), 7.75 (s, 1H, ArH), 7.20 (t, $J = 8.68$ Hz, 2H, ArH), 4.42-4.34 (m, 1H, cyclohex-CH), 2.29 (d, $J = 11.56$ Hz, 2H, cyclohex- CH_2), 1.99 (d, $J = 13.64$ Hz, 2H, cyclohex- CH_2), 1.88-1.78 (m, 3H, cyclohex- CH_2), 1.62-1.50 (m, 2H, cyclohex- CH_2), 1.40-1.27 (m, 1H, cyclohex- CH_2); $^{13}\text{C}\{^1\text{H}\}$ NMR (CDCl_3 , 100 MHz): δ (ppm) 164.5, 162.0, 149.1, 145.6, 142.1, 138.9, 138.0, 135.3, 133.5, 132.9, 130.7, 128.1, 128.0, 123.7, 120.0, 116.0, 115.8, 114.4, 113.3, 112.7 (ArC), 55.4 (CH), 33.6 (CH_2), 25.7 (CH_2), 25.5 (CH_2); MS (ESI): m/z 412.3 ($\text{M}^+ + 1$); Anal Calcd for $\text{C}_{25}\text{H}_{22}\text{FN}_5$: C, 72.97; H, 5.39; N, 17.02; found C, 72.72; H, 5.20; N, 16.85.

8-(1-Cyclohexyl-1H-benzo[d]imidazol-6-yl)-6-(thiophen-3-yl)imidazo[1,2-a]pyrazine (14): Light green solid; 125.43 mg, 83% yield; R_f 0.4 (40% ethylacetate in hexane); mp 180-183 °C; ^1H

NMR (CDCl₃, 400 MHz): δ (ppm) 9.13 (d, J = 0.96 Hz, 1H, ArH), 8.73 (dd, 2J = 8.68 Hz, 3J = 1.52 Hz, 1H, ArH), 8.32 (s, 1H, ArH), 8.08 (s, 1H, ArH), 8.02 (m, 1H, ArH), 7.94 (d, J = 8.60 Hz, 1H, ArH), 7.83 (d, J = 0.72 Hz, 1H, ArH), 7.73 (d, J = 0.64 Hz, 1H, ArH), 7.60 (dd, 2J = 5.04 Hz, 3J = 1.20 Hz, 1H, ArH), 7.45 (dd, 2J = 5.00 Hz, 3J = 3.08 Hz, 1H, ArH), 4.42-4.35 (m, 1H, cyclohex-CH), 2.30 (d, J = 12.08 Hz, 2H, cyclohex-CH₂), 1.99 (d, J = 10.96 Hz, 2H, cyclohex-CH₂), 1.88-1.78 (m, 3H, cyclohex-CH₂), 1.61-1.52 (m, 2H, cyclohex-CH₂), 1.39-1.28 (m, 1H, cyclohex-CH₂); ¹³C{¹H} NMR (CDCl₃, 100 MHz): δ (ppm) 149.3, 145.6, 142.0, 139.0, 138.9, 135.6, 135.1, 133.5, 130.7, 126.8, 125.1, 123.8, 123.0, 120.0, 114.3, 113.1, 112.6 (ArC), 55.4 (CH), 33.6 (CH₂), 25.7 (CH₂), 25.5 (CH₂); MS (ESI): m/z 400.2 (M⁺+1); Anal Calcd for C₂₃H₂₁N₅S: C, 69.15; H, 5.30; N, 17.53; S, 8.02; found C, 69.47; H, 5.59; N, 17.65; S, 8.40.

8-(1-Cyclohexyl-1H-benzo[d]imidazol-6-yl)-6-(*m*-tolyl)imidazo[1,2-*a*]pyrazine (**15**): Light green solid; 121.78 mg, 79% yield; R_f 0.6 (40% ethylacetate in hexane); mp 182-185 °C; ¹H NMR (CDCl₃, 400 MHz): δ (ppm) 9.16 (d, J = 1.04 Hz, 1H, ArH), 8.79 (dd, 2J = 8.64 Hz, 3J = 1.52 Hz, 1H, ArH), 8.41 (s, 1H, ArH), 8.08 (s, 1H, ArH), 7.95 (d, J = 8.60 Hz, 1H, ArH), 7.91 (s, 1H, ArH), 7.85 (s, 1H, ArH), 7.83 (s, 1H, ArH), 7.76 (s, 1H, ArH), 7.41 (t, J = 7.60 Hz, 1H, ArH), 7.22 (s, 1H, ArH), 4.43-4.35 (m, 1H, cyclohex-CH), 2.46 (s, 3H, CH₃), 2.31 (d, J = 11.44 Hz, 2H, cyclohex-CH₂), 2.00 (d, J = 13.56 Hz, 2H, cyclohex-CH₂), 1.89-1.79 (m, 3H, cyclohex-CH₂), 1.62-1.51 (m, 2H, cyclohex-CH₂), 1.42-1.31 (m, 1H, cyclohex-CH₂); ¹³C{¹H} NMR (CDCl₃, 100 MHz): δ (ppm) 149.0, 145.6, 142.0, 139.0, 139.0, 138.6, 136.7, 135.2, 133.5, 130.9, 129.5, 128.9, 127.1, 123.9, 123.4, 120.0, 114.3, 113.6, 112.6 (ArC), 55.4 (CH), 33.5 (CH₂), 25.7 (CH₂), 25.5 (CH₂), 21.6 (CH₃); MS (ESI): m/z 408.6 (M⁺+1); Anal Calcd for: C₂₆H₂₅N₅: C, 76.63; H, 6.18; N, 17.19; found C, 76.53; H, 6.14; N, 17.45.

8-(1-Cyclohexyl-1H-benzo[d]imidazol-6-yl)-6-(4-ethylphenyl)imidazo[1,2-*a*]pyrazine (**16**): Light green solid; 130.75 mg, 82% yield; R_f 0.6 (40% ethylacetate in hexane); mp 184-186 °C; ¹H NMR (CDCl₃, 400 MHz): δ (ppm) 9.16 (d, J = 0.76 Hz, 1H, ArH), 8.79 (dd, 2J = 8.60 Hz, 3J = 1.40 Hz, 1H, ArH), 8.39 (s, 1H, ArH), 8.08 (s, 1H, ArH), 8.00 (d, J = 8.16 Hz, 2H, ArH), 7.94 (d, J = 8.64 Hz, 1H, ArH), 7.84 (s, 1H, ArH), 7.75 (s, 1H, ArH), 7.35 (d, J = 8.12 Hz, 2H, ArH), 4.43-4.35 (m, 1H, cyclohex-CH), 2.75 (q, J = 7.60 Hz, 2H, CH₂), 2.31 (d, J = 11.60 Hz, 2H, cyclohex-CH₂), 2.00 (d, J = 13.56 Hz, 2H, cyclohex-CH₂), 1.89-1.78 (m, 3H, cyclohex-CH₂), 1.63-1.52 (m, 2H, cyclohex-CH₂), 1.40-1.30 (m, 1H, cyclohex-CH₂), 1.30 (t, J = 7.60 Hz, 3H, -CH₃); ¹³C{¹H} NMR (CDCl₃, 100 MHz): δ (ppm) 149.0, 145.5, 145.0, 141.9, 139.0, 135.1, 134.3, 133.5, 131.0, 128.5, 126.3, 123.9, 120.0, 114.2, 113.2, 112.6 (ArC), 55.4 (CH), 33.6 (CH₂), 28.7 (CH₂), 25.7 (CH₂), 25.5 (CH₂), 15.6 (CH₃); MS (ESI): m/z 422.5 (M⁺+1); Anal Calcd for C₂₇H₂₇N₅: C, 76.93; H, 6.46; N, 16.61; found C, 76.82; H, 6.31; N, 16.75.

1-(4-(8-(1-Cyclohexyl-1H-benzo[d]imidazol-6-yl)imidazo[1,2-*a*]pyrazin-6-yl)phenyl)ethan-1-one (**17**): Light green solid; 131.81 mg, 80% yield; R_f 0.6 (40% ethylacetate in hexane); mp 201-204 °C; ¹H NMR (CDCl₃, 400 MHz): δ (ppm) 9.21 (s, 1H, ArH), 8.78 (dd, 2J = 8.60 Hz, 3J = 1.16 Hz, 1H,

ArH), 8.53 (s, 1H, ArH), 8.20 (d, $J = 8.40$ Hz, 2H, ArH), 8.13 (s, 1H, ArH), 8.10 (d, $J = 8.40$ Hz, 2H, ArH), 7.96 (d, $J = 8.64$ Hz, 1H, ArH), 7.89 (s, 1H, ArH), 7.81 (s, 1H, ArH), 4.44-4.37 (m, 1H, cyclohex-CH), 2.66 (s, 3H, CH₃), 2.32 (d, $J = 12.32$ Hz, 2H, cyclohex-CH₂), 2.01 (d, $J = 13.80$ Hz, 2H, cyclohex-CH₂), 1.90-1.79 (m, 3H, cyclohex-CH₂), 1.63-1.53 (m, 2H, cyclohex-CH₂), 1.40-1.30 (m, 1H, cyclohex-CH₂); ¹³C{¹H} NMR (CDCl₃, 100 MHz): δ (ppm) 197.8 (C=O), 141.2, 139.0, 137.5, 136.9, 135.5, 130.9, 129.1, 126.3, 124.1, 119.7, 114.7, 112.9 (ArC), 55.6 (CH), 33.5 (CH₂), 26.8 (CH₃), 25.7 (CH₂), 25.4 (CH₂); MS (ESI): m/z 436.4 (M⁺+1); Anal Calcd for C₂₇H₂₅N₅O: C, 74.46; H, 5.79; N, 16.08; found C, 74.36; H, 5.89; N, 16.40.

6-(4-Chlorophenyl)-8-(1-cyclohexyl-1H-benzo[d]imidazol-6-yl)imidazo[1,2-a]pyrazine (18): Light green solid; 126.15 mg, 78% yield; R_f 0.6 (40% ethylacetate in hexane); mp 189-193 °C; ¹H NMR (CDCl₃, 400 MHz): δ (ppm) 9.18 (s, 1H, ArH), 8.74 (dd, $^2J = 8.64$ Hz, $^3J = 1.36$ Hz, 1H, ArH), 8.40 (s, 1H, ArH), 8.11 (s, 1H, ArH), 8.01 (d, $J = 8.56$ Hz, 2H, ArH), 7.94 (d, $J = 8.64$ Hz, 1H, ArH), 7.86 (d, $J = 0.60$ Hz, 1H, ArH), 7.76 (d, $J = 0.60$ Hz, 1H, ArH), 7.47 (s, 1H, ArH), 7.45 (s, 1H, ArH), 4.43-4.35 (m, 1H, cyclohex-CH), 2.30 (d, $J = 12.12$ Hz, 2H, cyclohex-CH₂), 2.00 (d, $J = 13.76$ Hz, 2H, cyclohex-CH₂), 1.88-1.76 (m, 3H, cyclohex-CH₂), 1.62-1.52 (m, 2H, Cyclohex-CH₂), 1.39-1.31 (m, 1H, Cyclohex-CH₂); ¹³C{¹H} NMR (CDCl₃, 100 MHz): δ (ppm) 149.1, 145.4, 142.0, 138.9, 137.7, 135.4, 135.3, 134.7, 133.4, 130.7, 129.1, 127.5, 123.8, 119.9, 114.5, 113.6, 112.7 (ArC), 55.5 (CH), 33.6 (CH₂), 25.7 (CH₂), 25.5 (CH₂); MS (ESI): m/z 428.4 (M⁺+1); Anal Calcd for C₂₅H₂₂ClN₅: C, 70.17; H, 5.18; N, 16.37; found C, 70.25; H, 5.14; N, 16.32.

6-(4-Bromophenyl)-8-(1-cyclohexyl-1H-benzo[d]imidazol-6-yl)imidazo[1,2-a]pyrazine (19): Light green solid; 139.44 mg, 78% yield; R_f 0.6 (40% ethylacetate in hexane); mp 197-200 °C; ¹H NMR (CDCl₃, 400 MHz): δ (ppm) 9.18 (s, 1H, ArH), 8.74 (dd, $^2J = 8.56$ Hz, $^3J = 1.40$ Hz, 1H, ArH), 8.39 (s, 1H, ArH), 8.12 (s, 1H, ArH), 7.94 (d, $J = 8.56$ Hz, 3H, ArH), 7.85 (s, 1H, ArH), 7.75 (s, 1H, ArH), 7.62 (d, $J = 8.52$ Hz, 2H, ArH), 4.42-4.35 (m, 1H, cyclohex-CH), 2.30 (d, $J = 12.60$ Hz, 2H, cyclohex-CH₂), 2.00 (d, $J = 13.68$ Hz, 2H, cyclohex-CH₂), 1.88-1.79 (m, 3H, cyclohex-CH₂), 1.61-1.51 (m, 2H, cyclohex-CH₂), 1.40-1.30 (m, 1H, cyclohex-CH₂); ¹³C{¹H} NMR (CDCl₃, 100 MHz): δ (ppm) 149.1, 138.9, 137.7, 135.7, 135.3, 132.0, 130.7, 128.6, 127.8, 127.4, 126.8, 123.8, 122.9, 119.9, 114.5, 113.6, 112.8 (ArC), 55.5 (CH), 33.5 (CH₂), 25.7 (CH₂), 25.5 (CH₂); MS (ESI): m/z 472.2 (M⁺+1); Anal Calcd for C₂₅H₂₂BrN₅: C, 63.57; H, 4.69; N, 14.83; found C, 63.27; H, 4.34; N, 14.95.

8-(1-Cyclohexyl-1H-benzo[d]imidazol-6-yl)-6-(2-methoxyphenyl)imidazo[1,2-a]pyrazine (20): Light green solid; 128.17 mg, 80% yield; R_f 0.5 (40% ethylacetate in hexane); mp 191-194 °C; ¹H NMR (CDCl₃, 400 MHz): δ (ppm) 9.14 (s, 1H, ArH), 8.86 (s, 1H, ArH), 8.76 (dd, $^2J = 8.64$ Hz, $^3J = 1.40$ Hz, 1H, ArH), 8.38 (dd, $^2J = 7.76$ Hz, $^3J = 1.76$ Hz, 1H, ArH), 8.12 (s, 1H, ArH), 7.94 (d, $J = 8.60$ Hz, 1H, ArH), 7.85 (d, $J = 1.04$ Hz, 1H, ArH), 7.76 (d, $J = 0.84$ Hz, 1H, ArH), 7.40-7.36 (m, 1H, ArH), 7.20-7.15 (m, 1H, ArH), 7.06 (d, $J = 8.24$ Hz, 1H, ArH), 4.44-4.36 (m, 1H, cyclohex-CH), 3.97 (s, 3H, CH₃), 2.31 (d, $J = 12.36$ Hz, 2H, cyclohex-CH₂), 2.00 (d, $J = 13.76$ Hz, 2H, cyclohex-CH₂),

1.88-1.78 (m, 3H, cyclohex-CH₂), 1.64-1.52 (m, 2H, cyclohex-CH₂), 1.40-1.32 (m, 1H, cyclohex-CH₂); ¹³C{¹H} NMR (CDCl₃, 100 MHz): δ (ppm) 156.8, 141.8, 138.8, 135.2, 135.0, 131.2, 131.0, 129.6, 125.3, 123.9, 121.3, 119.8, 118.4, 114.3, 112.4, 111.4 (ArC), 55.8 (CH), 55.4 (OCH₃), 33.6 (CH₂), 25.7 (CH₂), 25.5 (CH₂); MS (ESI): m/z 424.3 (M⁺+1); Anal Calcd for C₂₆H₂₅N₅O: C, 73.74; H, 5.95; N, 16.54; found C, 73.77; H, 5.72; N, 16.36.

8-(1-Cyclohexyl-1H-benzo[d]imidazol-6-yl)-6-(2-fluorophenyl)imidazo[1,2-a]pyrazine (21): Light green solid; 127.64 mg, 82% yield; R_f 0.4 (40% ethylacetate in hexane); mp 192-194 °C; ¹H NMR (CDCl₃, 400 MHz): δ (ppm) 9.20 (d, *J* = 0.92 Hz, 1H, ArH), 8.74 (dd, ²*J* = 8.56 Hz, ³*J* = 1.40 Hz, 1H, ArH), 8.67 (s, 1H, ArH), 8.46-8.41 (m, 1H, ArH), 8.13 (s, 1H, ArH), 7.95 (d, *J* = 8.64 Hz, 1H, ArH), 7.87 (s, 1H, ArH), 7.78 (s, 1H, ArH), 7.67-7.62 (m, 1H, ArH), 7.35-7.33 (m, 1H, ArH), 7.21-7.16 (m, 1H, ArH), 4.43-4.37 (m, 1H, cyclohex-CH), 2.31 (d, *J* = 12.12 Hz, 2H, cyclohex-CH₂), 2.00 (d, *J* = 13.80 Hz, 2H, cyclohex-CH₂), 1.89-1.79 (m, 3H, cyclohex-CH₂), 1.66-1.52 (m, 2H, cyclohex-CH₂), 1.43-1.32 (m, 1H, cyclohex-CH₂); ¹³C{¹H} NMR (CDCl₃, 100 MHz): δ (ppm) 149.1, 141.9, 138.8, 135.3, 133.4, 132.2, 132.1, 130.8, 130.0, 129.9, 128.6, 128.5, 124.8, 123.8, 119.9, 117.9, 117.8, 116.3, 116.1, 114.6, 112.8 (ArC), 55.5 (CH), 33.6 (CH₂), 25.7 (CH₂), 25.5 (CH₂); MS (ESI): m/z 412.3 (M⁺+1); Anal Calcd for C₂₅H₂₂FN₅: C, 72.97; H, 5.39; N, 17.02; found C, 72.73; H, 5.42; N, 17.42.

8-(1-Cyclohexyl-1H-benzo[d]imidazol-6-yl)-6-(thiophen-2-yl)imidazo[1,2-a]pyrazine (22): Light green solid; 123.92 mg, 82% yield; R_f 0.4 (40% ethylacetate in hexane); mp 188-191 °C; ¹H NMR (CDCl₃, 400 MHz): δ (ppm) 9.16 (s, 1H, ArH), 8.79 (dd, ²*J* = 8.64 Hz, ³*J* = 1.28 Hz, 1H, ArH), 8.34 (s, 1H, ArH), 8.10 (s, 1H, ArH), 7.93 (d, *J* = 8.64 Hz, 1H, ArH), 7.82 (s, 1H, ArH), 7.71 (s, 1H, ArH), 7.55 (d, *J* = 3.40 Hz, 1H, ArH), 7.38 (d, *J* = 5.00 Hz, 1H, ArH), 7.12 (q, *J* = 3.76 Hz, 1H, ArH), 4.41-4.34 (m, 1H, cyclohex-CH), 2.30 (d, *J* = 12.12 Hz, 2H, cyclohex-CH₂), 1.99 (d, *J* = 13.72 Hz, 2H, cyclohex-CH₂), 1.89-1.79 (m, 3H, cyclohex-CH₂), 1.66-1.47 (m, 2H, cyclohex-CH₂), 1.39-1.29 (m, 1H, cyclohex-CH₂); ¹³C{¹H} NMR (CDCl₃, 100 MHz): δ (ppm) 148.9, 145.4, 142.1, 141.9, 138.8, 135.3, 134.8, 133.4, 130.5, 128.1, 126.6, 124.0, 123.1, 119.8, 114.4, 112.7, 111.8 (ArC), 55.5 (CH), 33.5 (CH₂), 25.7 (CH₂), 25.5 (CH₂); MS (ESI): m/z 400.2 (M⁺+1); Anal Calcd for C₂₃H₂₁N₅S: C, 69.15; H, 5.30; N, 17.53; S, 8.02; found C, 69.14; H, 5.33; N, 17.32; S, 8.24.

8-(1-Cyclohexyl-1H-benzo[d]imidazol-6-yl)-6-(3-(trifluoromethyl)phenyl)imidazo[1,2-a]pyrazine (23): Light green solid; 148.42 mg, 85% yield; R_f 0.6 (40% ethylacetate in hexane); mp 198-201 °C; ¹H NMR (CDCl₃, 400 MHz): δ (ppm) 9.17 (s, 1H, ArH), 8.83 (dd, ²*J* = 8.64 Hz, ³*J* = 1.36 Hz, 1H, ArH), 8.50 (s, 1H, ArH), 8.37 (s, 1H, ArH), 8.26 (d, *J* = 7.60 Hz, 1H, ArH), 8.11 (s, 1H, ArH), 7.96 (d, *J* = 8.60 Hz, 1H, ArH), 7.89 (s, 1H, ArH), 7.80 (s, 1H, ArH), 7.70-7.61 (m, 2H, ArH), 4.43-4.35 (m, 1H, cyclohex-CH), 2.31 (d, *J* = 12.24 Hz, 2H, cyclohex-CH₂), 2.01 (d, *J* = 13.76 Hz, 2H, cyclohex-CH₂), 1.91-1.81 (m, 3H, cyclohex-CH₂), 1.65-1.62 (m, 2H, cyclohex-CH₂), 1.40-1.33 (m, 1H, cyclohex-CH₂); ¹³C{¹H} NMR (CDCl₃, 100 MHz): δ (ppm) 149.1, 142.1, 138.9, 137.6, 137.2,

135.5, 133.4, 131.2, 130.7, 129.4, 129.3, 125.2, 124.5, 124.1, 123.1, 119.7, 114.7, 114.1, 112.7 (ArC), 55.7 (CH), 33.5 (CH₂), 25.7 (CH₂), 25.4 (CH₂); MS (ESI): *m/z* 462.4 (M⁺+1); Anal Calcd for C₂₆H₂₂F₃N₅: C, 67.67; H, 4.81; N, 15.18; found C, 67.82; H, 4.99; N, 15.00.

8-(1-Benzyl-1H-benzo[d]imidazol-6-yl)-6-(4-ethylphenyl)imidazo[1,2-a]pyrazine (24): Light brown solid; 132.20 mg, 83% yield; *R_f* 0.3 (40% ethylacetate in hexane); mp 179-181 °C; ¹H NMR (CDCl₃, 400 MHz): δ (ppm) 9.08 (s, 1H, ArH), 8.83 (dd, ²*J* = 8.52 Hz, ³*J* = 1.44 Hz, 1H, ArH), 8.37 (s, 1H, ArH), 8.00 (s, 1H, ArH), 7.97-7.94 (m, 3H, ArH), 7.81 (s, 1H, ArH), 7.73 (s, 1H, ArH), 7.37-7.28 (m, 7H, ArH), 5.47 (s, 2H, benzyl-CH₂), 2.75 (q, *J* = 7.60 Hz, 2H, ethyl-CH₂), 1.31 (t, *J* = 7.64 Hz, 3H, ethyl-CH₃); ¹³C{¹H} NMR (CDCl₃, 100 MHz): δ (ppm) 148.7, 145.6, 145.0, 144.6, 138.9, 135.5, 135.0, 134.1, 131.5, 129.1, 128.5, 128.4, 127.7, 126.2, 124.1, 120.0, 114.3, 113.2, 112.4 (ArC), 49.1 (benzyl-CH₂), 28.7 (ethyl-CH₂), 15.7 (ethyl-CH₃); MS (ESI): *m/z* 430.6 (M⁺+1); Anal Calcd for C₂₈H₂₃N₅: C, 78.30; H, 5.40; N, 16.31; found C, 78.38; H, 5.28; N, 16.10.

*8-(1-Benzyl-1H-benzo[d]imidazol-6-yl)-6-(*m*-tolyl)imidazo[1,2-a]pyrazine (25)*: Light brown solid; 124.80 mg, 81% yield; *R_f* 0.3 (40% ethylacetate in hexane); mp 184-187 °C; ¹H NMR (CDCl₃, 400 MHz): δ (ppm) 9.08 (d, *J* = 1.12 Hz, 1H, ArH), 8.82 (dd, ²*J* = 8.64 Hz, ³*J* = 1.44 Hz, 1H, ArH), 8.40 (s, 1H, ArH), 8.01 (s, 1H, ArH), 7.98 (d, *J* = 8.60 Hz, 1H, ArH), 7.86 (s, 1H, ArH), 7.83 (s, 1H, ArH), 7.74 (s, 1H, ArH), 7.41-7.28 (m, 7H, ArH), 7.25 (d, *J* = 7.56 Hz, 1H, ArH), 5.49 (s, 2H, benzyl-CH₂), 2.47 (s, 3H, CH₃); ¹³C{¹H} NMR (CDCl₃, 100 MHz): δ (ppm) 148.8, 145.7, 144.6, 138.9, 138.6, 136.7, 135.5, 135.1, 134.1, 131.4, 129.5, 129.1, 128.8, 128.4, 127.6, 127.0, 124.1, 123.4, 120.1, 114.3, 113.7, 112.4 (ArC), 49.1 (benzyl-CH₂), 21.7 (CH₃); MS (ESI): *m/z* 416.5 (M⁺+1); Anal Calcd for C₂₇H₂₁N₅: C, 78.05; H, 5.09; N, 16.86; found C, 77.95; H, 5.02; N, 17.04.

4-(8-(1-Benzyl-1H-benzo[d]imidazol-6-yl)imidazo[1,2-a]pyrazin-6-yl)benzaldehyde (26): Light brown solid; 125.83 mg, 79% yield; *R_f* 0.3 (40% ethylacetate in hexane); mp 182-185 °C; ¹H NMR (CDCl₃, 400 MHz): δ (ppm) 10.09 (s, 1H, CHO), 9.11 (s, 1H, ArH), 8.83 (d, *J* = 8.48 Hz, 1H, ArH), 8.53 (s, 1H, ArH), 8.23 (d, *J* = 8.12 Hz, 2H, ArH), 8.04-7.95 (m, 4H, ArH), 7.87 (s, 1H, ArH), 7.79 (s, 1H, ArH), 7.38-7.30 (m, 5H, ArH), 5.50 (s, 2H, benzyl-CH₂); ¹³C{¹H} NMR (CDCl₃, 100 MHz): δ (ppm) 191.9 (CO), 144.8, 142.5, 138.9, 137.2, 136.2, 135.6, 135.4, 131.0, 130.3, 129.1, 128.4, 127.6, 126.6, 124.1, 120.2, 114.9, 114.7, 112.7 (ArC), 49.2 (benzyl-CH₂); MS (ESI): *m/z* 430.6 (M⁺+1); Anal Calcd for C₂₇H₁₉N₅O: C, 75.51; H, 4.46; N, 16.31; found C, 75.58; H, 4.50; N, 16.30.

8-(1-Benzyl-1H-benzo[d]imidazol-6-yl)-6-(naphthalen-1-yl)imidazo[1,2-a]pyrazine (27): Light brown solid; 137.30 mg, 82% yield; *R_f* 0.3 (40% ethylacetate in hexane); mp 183-186 °C; ¹H NMR (CDCl₃, 400 MHz): δ (ppm) 9.04 (d, *J* = 1.04 Hz, 1H, ArH), 8.81 (dd, ²*J* = 8.68 Hz, ³*J* = 1.56 Hz, 1H, ArH), 8.26 (s, 1H, ArH), 8.23 (d, *J* = 8.48 Hz, 1H, ArH), 7.98-7.90 (m, 6H, ArH), 7.78 (s, 1H, ArH), 7.67 (d, *J* = 6.92 Hz, 1H, ArH), 7.58-7.54 (m, 2H, ArH), 7.52-7.45 (m, 2H, ArH), 7.31-7.27 (m, 2H, ArH), 7.25-7.23 (m, 1H, ArH), 5.43 (s, 2H, benzyl-CH₂); ¹³C{¹H} NMR (CDCl₃, 100 MHz): δ (ppm) 148.8, 145.6, 144.7, 140.3, 138.7, 135.4, 135.2, 135.2, 134.1, 134.1, 131.8, 131.3, 129.4, 129.1, 128.5,

128.3, 127.7, 127.6, 126.6, 126.1, 125.8, 125.4, 124.3, 120.1, 117.3, 114.2, 112.4 (ArC), 49.1 (benzyl-CH₂); MS (ESI): m/z 452.5 (M⁺+1); Anal Calcd for C₃₀H₂₁N₅: C, 79.80; H, 4.69; N, 15.51; found C, 79.65; H, 4.55; N, 15.76.

1,4-Dibromo-2-nitrobenzene (29): Procedure for synthesis of 1,4-dibromo-2-nitrobenzene (**29**) is similar as that for the synthesis of 2,4-dibromo-1-nitrobenzene (**2**) using 1,4-dibromobenzene (**28**).

4-Bromo-N-cyclohexyl-2-nitroaniline (30): Procedure for synthesis of 4-bromo-*N*-cyclohexyl-2-nitroaniline (**30**) is similar as that for the synthesis of 5-bromo-*N*-cyclohexyl-2-nitroaniline (**3a**) using 1,4-dibromo-2-nitrobenzene (**29**). Yellow solid; 2.40 gm, 75% yield; R_f 0.3 (hexane); mp 93-96 °C; ¹H NMR (CDCl₃, 400 MHz): δ (ppm) 8.27 (d, *J* = 2.40 Hz, 1H, ArH), 8.12 (d, *J* = 7.08 Hz, 1H, NH), 7.44 (dd, ²*J* = 9.20 Hz, ³*J* = 2.32 Hz, 1H, ArH), 6.79 (d, *J* = 9.28 Hz, 1H, ArH), 3.52-3.44 (m, 1H, cyclohex-CH), 2.05-2.02 (m, 2H, cyclohex-CH₂), 1.81-1.74 (m, 2H, cyclohex-CH₂), 1.68-1.64 (m, 1H, cyclohex-CH₂), 1.47-1.25 (m, 5H, cyclohex-CH₂); ¹³C {¹H} NMR (CDCl₃, 100 MHz): δ (ppm) 143.7, 138.8, 136.1, 131.8, 129.0, 116.0, 114.8, 114.2, 105.8 (ArC), 51.2 (CH), 32.6 (CH₂), 25.5 (CH₂), 24.5 (CH₂).

5-bromo-N¹-cyclohexylbenzene-1,2-diamine (31a): 5-Bromo-*N*-cyclohexyl-2-nitroaniline (**3a**) (1 g, 3.34 mmol) and sodium dithionite (2.9 g, 16.72 mmol) were charged in THF:water (3:2) mixture. Ammonia solution (3 ml) was added to the reaction mixture at room temperature and further stirred for 1h. The reaction mixture was extracted with ethyl acetate. Ethyl acetate was dried over Na₂SO₄. Crude brown product was directly used for further reaction without purification.

4-bromo-N¹-cyclohexylbenzene-1,2-diamine (31b): Similar synthesis route has been adopted using 4-bromo-*N*-cyclohexyl-2-nitroaniline (**30**).

6-bromo-1-cyclohexyl-1H-benzo[d]imidazole (32a): 5-Bromo-*N*¹-cyclohexylbenzene-1,2-diamine (**31a**) (1 g, 3.71 mmol) was stirred with triethylorthoformate (0.550 g, 3.71 mmol) in acetic acid at room temperature for 10 min. Reaction mixture was quenched in water and further treated with NaHCO₃ to basify the reaction and extracted using chloroform. Sodium sulphate was used to dry the chloroform layer. Column chromatography was performed to purify the crude product with the help of hexane and ethyl acetate (3:7) as eluent.

5-bromo-1-cyclohexyl-1H-benzo[d]imidazole (32b): Similar synthesis route has been adopted using 4-bromo-*N*¹-cyclohexylbenzene-1,2-diamine (**31b**).

1-cyclohexyl-6-(4,4,5,5-tetramethyl-1,3,2-dioxaborolan-2-yl)-1H-benzo[d]imidazole (33a): 6-bromo-1-cyclohexyl-1H-benzo[d]imidazole (**32a**) (2 gm, 7.16 mmol), bis(pinacolato)diboron (2.19 gm, 8.60 mmol), potassium acetate (1.05 gm, 10.75 mmol) and palladium(II)bis(triphenylphosphine)dichloride (5.0 mol%) were added in 1,4-dioxane (20 mL). The reaction mixture was refluxed for the period of 12 h until aryl halide got completely consumed as determined by thin layer chromatography. Solvent of reaction was evaporated under reduced pressure followed by addition of 100 ml water to the reaction mixture. The crude product was extracted using chloroform (3 × 50 mL). Extract was

dried over anhydrous Na₂SO₄, filtered to obtain the crude product. Crude material was purified via column chromatography using ethyl acetate and hexane as solvent system to obtain desired reddish yellow product.

1-cyclohexyl-5-(4,4,5,5-tetramethyl-1,3,2-dioxaborolan-2-yl)-1H-benzo[d]imidazole (**33b**):

Similar synthesis route has been adopted using 5-bromo-1-cyclohexyl-1H-benzo[d]imidazole (**32b**).

6,8-(Bisbenzimidazole)imidazo[1,2-a]pyrazine (**34-36**): 1-Cyclohexyl-6-(4,4,5,5-tetramethyl-1,3,2-dioxaborolan-2-yl)-1H-benzo[d]imidazole (**33a**) or 1-cyclohexyl-5-(4,4,5,5-tetramethyl-1,3,2-dioxaborolan-2-yl)-1H-benzo[d]imidazole (**33b**) (1.0 eq), **8a-b** (1.0 eq., 150 mg), K₂CO₃ (1.0 eq.) and Pd(PPh₃)₄ (5 mol%) were taken in a mixture of acetonitrile : water (9:1). Reaction mixture was refluxed for 12-15 h under nitrogen until the completion of the reaction (checked by TLC). Solvents were evaporated under reduced pressure. Water (50 ml) was added to the mixture and extracted with chloroform. Chloroform layer was dried over sodium sulphate to get the crude product. Crude was further purified by column chromatography using hexane:ethylacetate as eluents.

6,8-Bis(1-cyclohexyl-1H-benzo[d]imidazol-6-yl)imidazo[1,2-a]pyrazine (**34**): Light brown solid; 152.15 mg, 78% yield; R_f 0.5 (40% ethylacetate in hexane); mp 225-228 °C; ¹H NMR (CDCl₃, 400 MHz): δ (ppm) 9.17 (d, *J* = 0.84 Hz, 1H, ArH), 8.75 (dd, ²*J* = 8.64 Hz, ³*J* = 1.36 Hz, 1H, ArH), 8.48 (s, 1H, ArH), 8.24 (s, 1H, ArH), 8.11 (s, 1H, ArH), 8.07 (s, 1H, ArH), 7.97 (d, *J* = 8.60 Hz, 1H, ArH), 7.91-7.84 (m, 3H, ArH), 7.80 (d, *J* = 0.72 Hz, 1H, ArH), 4.44-4.28 (m, 2H, 2 x cyclohex-CH), 2.27 (s (b), 4H, 2 x cyclohex-CH₂), 2.00 (d, *J* = 9.92 Hz, 4H, 2 x cyclohex-CH₂), 1.86-1.80 (m, 6H, 2 x cyclohex-CH₂), 1.61-1.51 (m, 4H, 2 x cyclohex-CH₂), 1.39-1.29 (m, 2H, 2 x cyclohex-CH₂); ¹³C{¹H} NMR (CDCl₃, 100 MHz): δ (ppm) 149.2, 149.2, 145.5, 144.2, 142.0, 141.5, 141.5, 139.5, 139.0, 135.3, 134.1, 133.5, 131.8, 130.9, 123.8, 120.6, 120.5, 120.0, 114.3, 113.7, 112.7, 108.7 (ArC), 55.5 (CH), 55.4 (CH), 33.6 (CH₂), 25.7 (CH₂), 25.7 (CH₂), 25.5 (CH₂), 25.4 (CH₂); MS (ESI): *m/z* 516.6 (M⁺+1); Anal Calcd for C₃₂H₃₃N₇: C, 74.54; H, 6.45; N, 19.01; found C, 74.65; H, 6.71; N, 19.32.

6-(1-Cyclohexyl-1H-benzo[d]imidazol-5-yl)-8-(1-cyclohexyl-1H-benzo[d]imidazol-6-yl)imidazo[1,2-a]pyrazine (**35**): Light brown solid; 146.30 mg, 75% yield; R_f 0.5 (80% ethylacetate in hexane); mp 204-207 °C; ¹H NMR (CDCl₃, 400 MHz): δ (ppm) 9.17 (s, 1H, ArH), 8.80 (dd, ²*J* = 8.68 Hz, ³*J* = 1.48 Hz, 1H, ArH), 8.47 (s, 1H, ArH), 8.45 (d, *J* = 1.00 Hz, 1H, ArH), 8.11-8.06 (m, 3H, ArH), 7.95 (d, *J* = 8.40 Hz, 1H, ArH), 7.86 (s, 1H, ArH), 7.79 (d, *J* = 0.64 Hz, 1H, ArH), 7.56 (d, *J* = 8.56 Hz, 1H, ArH), 4.44-4.34 (m, 1H, cyclohex-CH), 4.33-4.20 (m, 1H, cyclohex-CH), 2.31 (t, *J* = 12.80 Hz, 4H, 2 x cyclohex-CH₂), 2.00-1.97 (m, 4H, 2 x cyclohex-CH₂), 1.91-1.74 (m, 6H, 2 x cyclohex-CH₂), 1.65-1.48 (m, 4H, 2 x cyclohex-CH₂), 1.41-1.31 (m, 2H, 2 x cyclohex-CH₂); ¹³C{¹H} NMR (CDCl₃, 100 MHz): δ (ppm) 149.05, 145.45, 141.82, 141.46, 139.62, 139.02, 135.15, 133.93, 133.55, 131.47, 131.08, 124.00, 121.76, 119.97, 118.14, 114.39, 114.32, 113.39, 112.59, 110.58, 108.72, 77.42, 77.10, 76.79, 55.78, 55.34, 33.67, 33.42, 25.78, 25.74, 25.54, 25.48. (ArC), 55.7 (CH),

55.3 (CH), 33.6 (CH₂), 33.4 (CH₂), 25.7 (CH₂), 25.7 (CH₂), 25.5 (CH₂), 25.4 (CH₂); MS (ESI): m/z 516.6 (M⁺+1); Anal Calcd for C₃₂H₃₃N₇: C, 74.54; H, 6.45; N, 19.01; found C, 74.39; H, 6.38; N, 18.71.

8-(1-Benzyl-1H-benzo[d]imidazol-6-yl)-6-(1-cyclohexyl-1H-benzo[d]imidazol-5-yl)imidazo[1,2-a]pyrazine (36): Light green solid; 157.28 mg, 81% yield; R_f 0.5 (90% ethylacetate in hexane); mp 131-134 °C; ¹H NMR (CDCl₃, 400 MHz): δ (ppm) 9.13 (d, *J* = 1.12 Hz, 1H, ArH), 8.87 (dd, ²*J* = 8.64 Hz, ³*J* = 1.48 Hz, 1H, ArH), 8.45 (s, 2H, ArH), 8.07 (s, 1H, ArH), 8.06 (dd, ²*J* = 8.60 Hz, ³*J* = 1.60 Hz, 1H, ArH), 8.00 (s, 1H, ArH), 7.99 (d, *J* = 8.64 Hz, 1H, ArH), 7.83 (d, *J* = 0.84 Hz, 1H, ArH), 7.77 (s, 1H, ArH), 7.55 (d, *J* = 8.56 Hz, 1H, ArH), 7.38-7.28 (m, 5H, ArH), 5.50 (s, 2H, benzyl-CH₂), 4.28-4.20 (m, 1H, cyclohex-CH), 2.28 (d, *J* = 11.16 Hz, 2H, cyclohex-CH₂), 2.02 (d, *J* = 13.64 Hz, 2H, cyclohex-CH₂), 1.87-1.78 (m, 3H, cyclohex-CH₂), 1.59-1.49 (m, 2H, cyclohex-CH₂), 1.40-1.29 (m, 1H, cyclohex-CH₂); ¹³C{¹H} NMR (CDCl₃, 100 MHz): δ (ppm) 148.6, 145.5, 144.6, 144.3, 141.4, 139.4, 138.9, 135.5, 135.0, 134.2, 133.9, 131.5, 131.3, 129.1, 128.4, 127.7, 124.2, 121.6, 120.0, 118.1, 114.3, 113.3, 112.4, 110.5 (ArC), 55.7 (CH), 49.0 (benzyl-CH₂), 33.4 (CH₂), 25.7 (CH₂), 25.4 (CH₂); MS (ESI): m/z 524.6 (M⁺+1); Anal Calcd for C₃₃H₂₉N₇: C, 75.69; H, 5.58; N, 18.72; found C, 75.63; H, 5.63; N, 18.75.

Procedure for in vitro anticancer screening

The human tumor cell lines of the cancer screening panel are grown in RPMI 1640 medium containing 5% fetal bovine serum and 2 mM L-glutamine. Cells are inoculated into 96 well microtiter plates in 100 μl at plating densities ranging from 5,000 to 40,000 cells/well depending on the doubling time of individual cell lines. The microtiter plates are then incubated at 37 °C, 5% CO₂, 95% air and 100% relative humidity for 24 h.

After 24 h, two plates of each cell line are fixed in situ with TCA, to represent a measurement of the cell population for each cell line. Experimental drugs are solubilized in DMSO at 400-fold the desired final maximum test concentration and stored frozen prior to use. At the time of drug addition, an aliquot of frozen concentrate is thawed and diluted to twice the desired final maximum test concentration with complete medium containing 50 μg/ml gentamicin. Additional four, 10-fold or ½ log serial dilutions are made to provide a total of five drug concentrations plus control. Aliquots of 100 μL of these different drug dilutions are added to the appropriate microtiter wells, resulting in the required final drug concentrations. Following drug addition, the plates are incubated for an additional 48 h at 37 °C, 5% CO₂, 95% air, and 100% relative humidity. For adherent cells, the assay is terminated by the addition of cold TCA. Cells are fixed in situ by the gentle addition of 50 μL of cold 50% (w/v) TCA and incubated for 60 min at 4 °C. The supernatant is discarded, and the plates are washed five times with tap water and air dried. Sulforhodamine B (SRB) solution (100 μL) at 0.4% (w/v) in 1% acetic acid is added to each well, and plates are incubated for 10 min at room temperature. After staining, unbound dye is removed by washing five times with 1% acetic acid and the plates are air dried and then subsequently solubilized with 10 mM trizma base, and the absorbance

is read on an automated plate reader at a wavelength of 515 nm. Using the seven absorbance measurements [time zero (T_z), control growth (C), and test growth in the presence of drug at the five concentration levels (T_i)], the percentage growth is calculated at each of the drug concentration levels. Percentage growth inhibition is calculated as:

$[(T_i - T_z)/(C - T_z)] \times 100$ for concentrations for which $T_i \geq T_z$; $[(T_i - T_z)/T_z] \times 100$ for concentrations for which $T_i < T_z$.

Three dose response parameters are calculated for each experimental agent. Growth inhibition of 50% (GI_{50}) is calculated from $[(T_i - T_z)/(C - T_z)] \times 100 = 50$. The drug concentration resulting in total growth inhibition (TGI) is calculated from $T_i = T_z$. The LC_{50} is calculated from $[(T_i - T_z)/T_z] \times 100 = 50$.

Cytotoxicity against human normal cell line. Hek293 (Human embryonic kidney) cells were cultured in DMEM with 50 mM glutamine, 10% FBS, 100 U/ml penicillin and 100 mg/ml streptomycin. Cells were seeded in two different 96 well plates at the density of 1×10^5 cells/well in DMEM media supplemented with 10% FBS cells. Cells were incubated at 37 °C in 5% CO_2 incubator. Cells were treated with compound **8** at five concentrations (10^{-4} , 10^{-5} , 10^{-6} , 10^{-7} , 10^{-8} M) at 37 °C for 48 h. 10 μ l of MTT (prepared in 1* PBS buffer) from 5 mg/ml stock was added in each well and incubated at 37 °C for 4 h in dark. The formazan crystals were dissolved using 100 μ l of DMSO. Further, the amount of formazan crystal formation was measured as difference in absorbance by Bio-Tek ELISA plate reader at 570 nm reference wavelength. All experiments were independently performed at least three times. The relative cell toxicity (%) related to control wells containing culture medium without test material was calculated by using formula:

$$\% \text{ Cell Toxicity} = 100 - \frac{\text{OD (Compound treated wells)}}{\text{OD (Untreated Wells)}} \times 100$$

DNA and BSA interaction studies.

Sample preparation. The stock solution of calf thymus (ct)-DNA was prepared by dissolving the DNA in 10 mM Tris with 1 mM EDTA (pH 7.4) at room temperature. Ratio of absorbance at 260 nm to 280 nm was used to calculate the purity of DNA solution. Concentration of stock solution of DNA was measured taking average extinction coefficient $6600 \text{ M}^{-1} \text{ cm}^{-1}$ of a single nucleotide at 260 nm.

The stock solutions (10^{-3} M) of compounds (**10** and **36**) and BSA were prepared in DMSO and distilled water, respectively.

UV-visible spectroscopic method. The compounds (**10** and **36**) (20 μ M, phosphate buffer pH 7.4) were titrated with incremental addition of ct-DNA (**10**; 0-10 μ M and **36**; 0-12 μ M).

The experiment for BSA interaction with compounds (**10** and **36**) was performed taking BSA (10 μ M, phosphate buffer, pH 7.4) and incremental addition of compounds (0-8 μ M).

In both ct-DNA and BSA interactions studies, base line corrections were carried out using blank solution containing phosphate buffer and UV-visible spectra were noted in the range of 200–800 nm. Binding constants (K_b) were determined from Benesi-Hildebrand equation (equation-1).

$$\frac{A_0}{(A-A_0)} = \frac{\epsilon_f}{(\epsilon_b - \epsilon_f)} + \frac{\epsilon_f}{(\epsilon_b - \epsilon_f) K_b [\text{Analyte}]} \text{-----} 1$$

Where A_0 is the initial absorbance of the free compound/BSA, A is the absorbance of the compound/BSA in the presence of analyte (ct-DNA or compound), ϵ_f and ϵ_b are molar extinction coefficients of the compound or BSA in its free and fully bound forms, respectively. The plot of $A_0/(A-A_0)$ versus $1/[\text{analyte}]$ was constructed using the titration data and linear fitting, and the value of K_b is determined taking ratio of the intercept to the slope.

DNA melting studies. DNA melting experiments were performed by recording the absorption of ct-DNA (8.5 μM) and complex of ct-DNA (8.5 μM) with compounds (**10** and **36**) (10 μM) at the wavelength of 260 nm at different temperatures with the spectrophotometer attached with peltier. Melting temperature of the DNA (T_m) was calculated to be the transition midpoint.

Fluorescence studies. For ct-DNA studies, fluorescence emission spectra of compounds **10** and **36** were recorded upon excitation at **10**; 280 nm, **36**; 290 nm. The emission intensity of compounds **10** and **36** (5 μM) was recorded with varying concentration of ct-DNA (**10**; 0-110 μM , **36**; 0-40 μM) at 298 K. Emission spectra for compound **10** were also recorded at 308 K and 318 K.

For BSA studies, fluorescence spectral measurements were carried out for BSA (10 μM) with varying concentration of compounds (a) **10**: 0-10 μM and (b) **36**: 0-10 μM at 298 K.

All emission spectra for DNA and BSA studies were noted in the range of 200 to 800 nm. The excitation and emission slit widths have been maintained constant throughout the experiment. Stern-Volmer equation (equation-2) was used to find quenching process and to calculate the quenching constants

$$\frac{F_0}{F} = 1 + K_{sv} [\text{Analyte}] = 1 + K_q \tau_0 [\text{Analyte}] \text{-----} 2$$

Where F_0 and F are the intensities of emission spectra of compounds/BSA in the absence (free form) and presence of analyte (ct-DNA or compound), respectively. The Stern-Volmer quenching constant (K_{sv}) which is considered to be a measure of efficiency of fluorescence quenching by analyte and bimolecular quenching constants (K_q) were calculated from plot of F_0/F versus [analyte].

Modified Stern-Volmer equation (equation-3) was used to get the values of the binding constant (K_b) and the average number of binding sites (n).

$$\log \frac{F_0 - F}{F} = \log K_b + n \log [\text{analyte}] \text{-----} 3$$

The parameters are same as those of the Stern-Volmer equation. The binding constants (K_b) and the average number of binding sites (n) were calculated from antilog of intercept and slope of the straight regression line respectively, from the plot of $\log \{(F_0 - F)/F$ versus $\log [\text{analyte}]\}$.

To calculate the thermodynamic parameters i.e. the enthalpy change (ΔH) and entropy change (ΔS) the van't Hoff equation (equation-4) was used.

$$\log K_b = - \frac{\Delta H}{2.303RT} + \frac{\Delta S}{2.303R} \text{-----} 4$$

Where K_b , T and R are the binding constant, absolute temperature and gas constant, respectively. In addition, the free energy change (ΔG) for the binding of analyte at different temperatures was calculated using the following equation (equation-5).

$$\Delta G = \Delta H - T\Delta S \text{-----} 5$$

Competitive displacement assays. Ethidium bromide (EB) displacement assay was carried out by adding ligand to EB-DNA complex solution. The ethidium bromide ($3 \mu\text{M}$) and DNA ($30 \mu\text{M}$) were titrated with varying concentration of ligand ($0\text{--}85 \mu\text{M}$). The EB-DNA complex was excited at 520 nm and emission spectra were recorded between 200 nm and 800 nm .

Circular dichroism (CD) studies. CD spectra of ct-DNA ($40 \mu\text{M}$) alone and complex (ct-DNA and ligand at ratio of $r(\text{ligand};\text{ct-DNA}) = 0.025$) were recorded using an applied photophysics CD spectrophotometer. All the CD spectra were recorded in a range from 220 nm to 400 nm . The average of four scans was taken in all the experiments. The background spectrum of buffer solution (10 mM Tris-HCl, $\text{pH } 7.4$) was subtracted from the spectra of DNA and the ligand–DNA complex.

Shake-flask method

Partition coefficient of derivatives **9-27** and **34-36** were measured with *n*-octanol–phosphate buffer (0.15 M , $\text{pH} = 7.4$) at volumes of $10:1$. Stock solutions of all the derivatives were made in dimethylsulfoxide (HPLC grade) at 10^{-3} M concentration. All solutions throughout the experiment were prepared in glass vials; stock solution and phosphate buffer ($250 \mu\text{L}$, $125 \mu\text{L}$) were added to the glass vial using micropipette. The wavelength was chosen according to the λ_{max} of derivative. Initial absorbance (A_i) of each derivative was recorded using stock solution in the buffer phase. Then, *n*-octanol was added to the each glass vial and shaken together on a mechanical shaker (METREX, Cat No. MRS-50H) for 50 minutes. All glass vials were centrifuged (REMI R-24) at 2500 rpm for 35 minutes to get thoroughly separation of both phases. Octanol layer was removed from the vial and final absorbance (A_f) of the buffer layer was recorded.

P values for all derivatives were calculated using following equation (equation-6)-

$$P = \frac{A_i - A_f}{A_f} \times \frac{V_w}{V_o} \text{-----} 6$$

Where V_w and V_o denote the volume of the aqueous phase and organic phase, respectively.

Docking Simulation

Molecular docking of the complexes into 3-D X-ray structure of DNA (PdB: 1BNA) was carried out using the AutoDock software package (vina). The ligand structures in docking protocol were used as a crystal structure. The graphical user interface AutoDockTools (1.5.6rc3) was performed to setup

every ligand DNA interaction, where water molecules were deleted and polar hydrogen atoms were added, gasteiger charges were calculated. The 3D structures of the ligand molecules were optimized using Gaussian 09W program and saved in pdb format. The partial charges of pdb file were further modified by using the ADT package (version 1.5.6rc3), so that the charges of the nonpolar hydrogen atoms would be assigned to the atom to which the hydrogen is attached. The resulting file was saved as Pdbqt file. The AutoDockTools program was used to generate the docking put files. In all docking, a grid box size of 44, 78, 106 pointing in x, y and z directions were built. A grid spacing of 0.375 Å was used. Default settings were used with an initial population.

Acknowledgments

KP thanks the DST-SERB, New Delhi (EMR/2014/000669). IS is grateful for CSIR (Project No. 09/677(0033)/2018-EMR-I) for SRF. NIH, Bethesda, USA for anticancer activities, SAI labs, TIET for NMR are also acknowledged. Author thank to Punjab University, Chandigarh and IIT Ropar for providing mass facility and Dr Kamlesh Kumar, BHU, for solving the crystal structure.

Corresponding author

E-mail kpaul@thapar.edu

Notes

The authors declare no competing financial interest.

References

- [1] W. O. Foye, *Cancer Chemotherapeutic Agents*. American Chemical Society, Washington, DC, **1995**, ISBN: 0-8412-2920-1.
- [2] A. Mukherjee, W. D. Sasikala, Chapter one - Drug–DNA intercalation: From discovery to the molecular mechanism, *Adv. Protein Chem. Struct., Biol.*, **2013**, *92*, 1-62.
- [3] K. Xu, P. M. Schwarz, R. F. Ludueña, Interaction of nocodazole with tubulin isotypes, *Drug Dev. Res.*, **2002**, *55*, 91–96.
- [4] (a) L. A. Hammond, K. Davidson, R. Lawrence, J. B. Camden, D. D. Von Hoff, S. Weitman, E. Izbiccka, Exploring the mechanisms of action of FB642 at the cellular level, *J. Cancer Res. Clin. Oncol.*, **2001**, *127*, 301–313; (b) D. Hao, J. D. Rizzo, S. Stringer, R. V. Moore, J. Marty, D. L. Dexter, G. L. Mangold, J. B. Camden, D. D. Von Hoff, S. D. Weitman, Preclinical antitumor activity and pharmacokinetics of methyl-2-benzimidazolecarbamate (FB642), *Invest. New. Drugs*, **2000**, *20*, 261–270.
- [5] C. K. Donawho, Y. Luo, Y. Luo, T. D. Penning, J. L. Bauch, J. J. Bouska, V. D. Bontcheva-Diaz, B. F. Cox, T. L. DeWeese, L. E. Dillehay, D. C. Ferguson, N. S. Ghoreishi-Haack, D. R. Grimm, R. Guan, E. K. Han, R. R. Holley-Shanks, B. Hristov, K. B. Idler, K. Jarvis, E. F. Johnson, L. R. Kleinberg, V. Klinghofer, L. M. Lasko, X. Liu, K. C. Marsh, T. P. McGonigal, J. A. Meulbroek, A. M. Olson, J. P. Palma, L. E. Rodriguez, Y. Shi, J. A. Stavropoulos, A. C. Tsurutani, G. D. Zhu, S. H. Rosenberg, V. L. Giranda, D. J. Frost, ABT-888, an orally active

- poly(ADP-Ribose) polymerase inhibitor that potentiates DNA-damaging agents in preclinical tumor models, *Clin. Cancer Res.*, **2007**, *13*, 2728–2737.
- [6] P. Pantziarka, G. Bouche, L. Meheus, V. Sukhatme, V. P. Sukhatme, Repurposing drugs in oncology (ReDO)-mebendazole as an anti-cancer agent, *ecancermedicalsecience*, **2014**, *8*, 443-459.
- [7] M. Hegde, K. S. S. Kumar, E. Thomas, E. Ananda, S. C. Raghavan, K. S. Rangappa, A novel benzimidazole derivative binds to the DNA minor groove and induces apoptosis in leukemic cells, *RSC Adv.*, **2015**, *5*, 93194-93208.
- [8] A. S. Alpan, S. Zencir, I. Zupkó, G. Coban, B. Réthy, H. S. Gunes, Z. Topcu, Biological activity of bis-benzimidazole derivatives on DNA topoisomerase I and HeLa, MCF7 and A431 cells, *J. Enzyme Inhib. Med. Chem.*, **2009**, *24*, 844–849.
- [9] B. Maji, K. Kumar, M. Kaulage, K. Muniyappa, S. Bhattacharya, Design and synthesis of new benzimidazole-carbazole conjugates for the stabilization of human telomeric DNA, telomerase inhibition, and their selective action on cancer cells, *J. Med. Chem.*, **2014**, *57*, 6973–6988.
- [10] K. Paul, A. Sharma, V. Luxami, Synthesis and in vitro antitumor evaluation of primary amine substituted quinazoline linked benzimidazole, *Bioorg. Med. Chem. Lett.* **2014**, *24*, 624–629.
- [11] P. Singla, V. Luxami, K. Paul, Synthesis, in vitro antitumor activity, dihydrofolate reductase inhibition, DNA intercalation and structure–activity relationship studies of 1,3,5-triazine analogues, *Bioorg. Med. Chem. Lett.* **2016**, *26*, 518–523.
- [12] A. Sharma, V. Luxami, K. Paul, Purine-benzimidazole hybrids: Synthesis, single crystal determination and in vitro evaluation of antitumor activities, *Eur. J. Med. Chem.*, **2015**, *93*, 414-422.
- [13] M. Verma, V. Luxami, K. Paul, Synthesis, in vitro evaluation and molecular modelling of naphthalimide analogue as anticancer agents, *Eur. J. Med. Chem.*, **2013**, *68*, 352-360.
- [14] V. A. Sontakke, A. N. Kate, S. Ghosh, P. More, R. Gonnade, N. M. Kumbhar, A. A. Kumbhar, B. A. Chopade, V. S. Shinde, Synthesis, DNA interaction and anticancer activity of 2-anthryl substituted benzimidazole derivatives, *New J. Chem.*, **2015**, *39*, 4882-4890.
- [15] A. T. Baviskar, C. Madaan, R. Preet, P. Mohapatra, V. Jain, A. Agarwal, S. Guchhait, C. N. Kundu, U. C. Banerjee, P. V. Bharatam, *N*-Fused imidazoles as novel anticancer agents that inhibit catalytic activity of topoisomerase II α and induce apoptosis in G1/S phase, *J. Med. Chem.*, **2011**, *54*, 5013–5030.
- [16] A. Belatik, S. Hotchandani, J. Bariyanga, H. A. Tajmir-Riahi, Binding sites of retinol and retinoic acid with serum albumins, *Eur. J. Med. Chem.*, **2012**, *48*, 114-123.
- [17] G. T. Luc, L. G. T. Morris, T. A. Chan, Therapeutic targeting of tumor suppressor genes, *cancer*, **2015**, *121*, 1357–1368.

- [18] (a) R. Goel, V. Luxami, K. Paul, Palladium catalyzed novel monoarylation and symmetrical/unsymmetrical diarylation of imidazo[1,2-*a*]pyrazines and their *in vitro* anticancer activities, *RSC Adv.*, **2014**, *19*, 9885-9892; (b) H. Zeng, D. B. Belanger, P. J. Curran, G. W. Shipps Jr, H. Miao, J. B. Bracken, M. A. Siddiqui, M. Malkowski, Y. Wang, Discovery of novel imidazo[1,2-*a*]pyrazin-8-amines as Brk/PTK6 inhibitors, *Bioorg. Med. Chem. Lett.*, **2011**, *21*, 5870–5875.
- [19] C. A. Lipinski, F. Lombardo, B. W. Dominy, P. J. Feeney, Experimental and computational approaches to estimate solubility and permeability in drug discovery and development settings, *Adv. Drug Deliv. Rev.*, **1997**, *23*, 3-25.
- [20] P. Ertl, B. Rodhe, P. Selzer, Fast calculation of molecular polar surface areas as a sum of fragment based contribution and its application to the prediction of drug transport properties, *J. Med. Chem.*, **2000**, *43*, 3714-3717.
- [21] S. Prasanna, R. J. Doerksen, Topological polar surface area: a useful descriptor in 2D-QSAR, *Curr. Med. Chem.*, **2009**, *16*, 21-41.
- [22] (a) M. R. Grever, S. A. Sehepartz, B. A. Chabners, *Semin. Oncol.* **1992**, *19*, 622-638; (b) A. Monks, D. Schudiero, P. Skehan, R. Shoemaker, K. Paull, D. Vistica, C. Hose, J. Langley, P. Cronise, A. Vaigro-Wolff, M. Gray-Goodrich, H. Campbell, J. Mayo, M. J. Boyd, *Natl. Cancer Inst.* **1991**, *83*, 757-766; (c) Boyd, M. R.; Paull, K. D. *Drug Dev. Res.* **1995**, *34*, 91-109.
- [23] F. Arjmand, M. Aziz, Synthesis and characterization of dinuclear macrocyclic cobalt (II), copper (II) and zinc (II) complexes derived from 2,2,20,20-S,S[bis(bis-N,N-2-thiobenzimidazoloxalato-1,2-ethane)]: DNA binding and cleavage studies, *Eur. J. Med. Chem.*, **2009**, *44*, 834-844.
- [24] H. A. Benesi, J. H. Hildebrand, A spectrophotometric investigation of the interaction of iodine with aromatic hydrocarbons, *J. Am. Chem. Soc.*, **1949**, *71*, 2703–2707.
- [25] R. Palchaudhuri, P. J. Hergenrother, DNA as a target for anticancer compounds: Methods to determine the mode of binding and the mechanism of action, *Curr. Opin. Biotechnol.*, **2007**, *18*, 497-503.
- [26] M. R. Eftink, C. A. Ghiron, Fluorescence quenching studies with proteins, *Anal. Biochem.*, **1981**, *114*, 199-227.
- [27] J. R. Lakowicz, G. Weber, Quenching of protein fluorescence by oxygen. Detection of structural fluctuations in proteins on the nanosecond time scale, *Biochemistry*, **1973**, *12*, 4171-4179.
- [28] J. R. Lakowicz, G. Webber, Quenching of fluorescence by oxygen. Probe for structural fluctuations in macromolecules, *Biochemistry*, **1973**, *12*, 4161-4170.
- [29] (a) I. Parveen, P. Khan, S. Ali, I. Md. Hassan, N. Ahmed, Synthesis, molecular docking and inhibition studies of novel 3-*N*-aryl substituted-2-heteroarylchromones targeting microtubule

- affinity regulating kinase 4 inhibitors, *Eur. J. Med. Chem.* **2018**, *159*, 166-177; (b) P. Bourassa, S. Dubeau, G. M. Maharvi, A. H. Fauq, T. J. Thomas, H. A. Tajmir-Riahi, Locating the binding sites of anticancer tamoxifen and its metabolites 4-hydroxytamoxifen and endoxifen on bovine serum albumin, *Eur. J. Med. Chem.* **2011**, *46*, 4344-4353.
- [30] I. Haq, Thermodynamics of drug–DNA interactions, *Arch. Biochem. Biophys.*, **2002**, *403*, 1-15.
- [31] J. B. Lepecq, C. Paoletti, A fluorescent complex between ethidium bromide and nucleic acids physical-chemical characterization, *J. Mol. Biol.*, **1967**, *27*, 87-106.
- [32] M. Eriksson, B. Nordén, Linear and circular dichroism of drug-nucleic acid complexes, *Methods Enzymol.*, **2001**, *340*, 68-98
- [33] A. Rodger, B. Norden, In circular dichroism and linear dichroism, Oxford University Press, New York, **1997**, Chapter 2.
- [34] N. Berova, K. Nakanishi, R. W. Woody, Circular dichroism principles and applications, 2nd ed., Wiley-VCH, New York, **2000**.
- [35] M. Mohamadi, S. Y. Ebrahimipour, M. Torkzadeh-Mahani, S. Foro, A. Akbari, A mononuclear diketone-based oxido-vanadium(IV) complex: structure, DNA and BSA binding, molecular docking and anticancer activities against MCF-7, HPG-2, and HT-29 cell lines, *RSC Adv.*, **2015**, *5*, 101063-101075.
- [36] S. Fortli, R. Huey, M. E. Pique, M. Sanner, D. S. Goodsele, A. J. Olson, Computational protein-ligand docking and virtual drug screening with the AutoDock suite. *Nat. Protoc.*, **2016**, *11*, 905-919.
- [37] T. Sarwar, M. A. Husain, S. Ur Rehman, H. M. Ishqi, M. Tabish, Multi-spectroscopic and molecular modelling studies on the interaction of esculetin with calf thymus DNA. *Mol. Biosyst.* **2015**, *11*, 522-531.
- [38] F. Maya, J. M. Tour, Synthesis of terphenyl oligomers as molecular electronic device candidates. *Tetrahedron*, **2004**, *60*, 81-92.

Highlights

- A new series of imidazo[1,2-*a*]pyrazine-benzimidazole conjugates has been synthesized.
- Single X-ray crystal determination of compound **9**
- *In vitro* evaluation of synthesized compounds for their antitumor activity.
- Mode of interactions was studied with ct-DNA.
- Transportation of derivative was studied with bovine serum albumin.